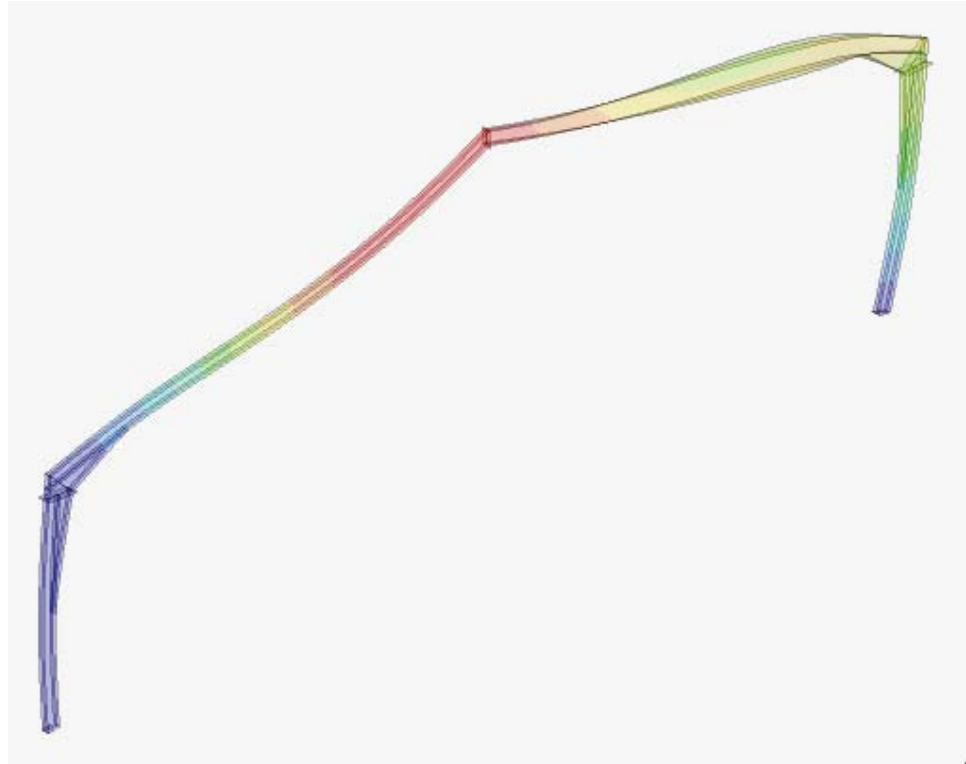




LUND
UNIVERSITY



DESIGN TOOLS FOR STEEL FRAMES

Challenges regarding stability

MELANIE DESHAYES and TRULS SOLLI LARSSON

Structural
Mechanics

Master's Dissertation

DEPARTMENT OF CONSTRUCTION SCIENCES
DIVISION OF STRUCTURAL MECHANICS

ISRN LUTVDG/TVSM--24/5273--SE (1-73) | ISSN 0281-6679

MASTER'S DISSERTATION

DESIGN TOOLS FOR STEEL FRAMES

Challenges regarding stability

MELANIE DESHAYES and TRULS SOLLI LARSSON

Supervisors: Professor **KENT PERSSON**, Division of Structural Mechanics, LTH
together with **MIKAEL FREDENBERG** and **MARTIN ERIKSSON**, FS Dynamics.
Examiner: **HENRIK DANIELSSON**, Associate Professor, Division of Structural Mechanics, LTH.

Copyright © 2024 Division of Structural Mechanics,
Faculty of Engineering LTH, Lund University, Sweden.
Printed by V-husets tryckeri LTH, Lund, Sweden, June 2024 (*PI*).

For information, address:
Division of Structural Mechanics,
Faculty of Engineering LTH, Lund University, Box 118, SE-221 00 Lund, Sweden.
Homepage: www.byggmek.lth.se

Abstract

When designing steel frames used in large hall buildings it is favourable to use a design tool set up with a programming language that can consider many different load cases and load combinations. These design tools can use the finite element method in order to perform the calculations needed to design the frames. Due to the extent of these design tools, the amount of elements used are restricted to a smaller number in order to have a low computational time. In this study one design tool, using a two-dimensional model with few beam elements, is investigated. A three-dimensional model of two frames with beam-profiles of IPE, one with and one without haunches, with many shell elements is created. A linear static, linear buckling and a non-linear static analysis is performed, for one load case and combination, in order to compare with the two-dimensional model regarding cross-section forces, displacements and stability of the structure.

With the linear static analysis, it is found that the two-dimensional model is sufficient to use when calculating cross-section forces and displacements. The implementation of haunches can be improved to more accurately model the stiffness of the corners. The linear and non-linear static analysis found that the design tool is insufficient when calculating the utilization in regards to stability according to European standards for designing buildings, Eurocode. For the load case and combination investigated both models established that lateral torsional buckling of the right beam was the cause for instability of the frame. The design tool conservatively calculates the critical load with a factor of 2 to 6.5 depending on the frame and analysis type. This conservatism is caused by estimates in Eurocode and in the two-dimensional model.

This thesis found that considering the moment distribution when calculating the utilization in regards to stability according to Eurocode will result in less conservative calculations. For the frame without haunches, the utilization was similar to the one derived from the non-linear analysis performed on the three-dimensional model. For the frame with haunches, the contribution to stability from the haunches needs to be implemented in order to have more accurate results.

The rigid connections between beams and purlins were modelled to investigate if the increased rotational stiffness, for the points where the purlins were attached to the beams, would assist in stabilizing the frame. This study found that modelling the connections as they are today will not contribute to increased stability. If the connections between purlins and beams improved from one-bolt connections to two-bolt connections, it would be of interest to incorporate this in the design tool.

Sammanfattning

Vid dimensionering av stålramar som används i stora hallbyggnader är det fördelaktigt att använda ett dimensioneringsverktyg, uppbyggt med hjälp av ett programmeringsspråk, som kan ta hänsyn till flera olika lastfall och lastkombinationer. Dessa dimensioneringsverktyg kan använda finita elementmetoden för att utföra de beräkningar som behövs för att dimensionera ramarna. På grund av omfattningen av dessa dimensioneringsverktyg är mängden element som används begränsad till ett mindre antal för att få en låg beräkningstid. I denna studie undersöks ett dimensioneringsverktyg som använder en tvådimensionell modell med få balkelement. En tredimensionell modell av två ramar med balkprofiler av IPE, en med och en utan voter, med många skalelement skapas. En linjär statisk, en linjär knäckning och en olinjär statisk analys utförs, för ett lastfall och en lastkombination, för att jämföra med den tvådimensionella modellen med avseende på snittkrafter, förskjutningar och stabilitet.

Den linjära statistiska analysen visar att den tvådimensionella modellen är tillräcklig för att använda vid beräkning av snittkrafter och förskjutningar. Implementeringen av hörn kan förbättras för att mer exakt modellera hörnens styvhet. Den linjära och olinjära statistiska analysen visade att dimensioneringsverktyget är otillräckligt vid beräkning av utnyttjandegraden med avseende på stabilitet enligt europeisk standard för dimensionering av byggnader, Eurokod. För det undersökta lastfallet och lastkombinationen visade båda modellerna att vippning av den högra balken var orsaken till ramens instabilitet. Dimensioneringsverktyget beräknar den kritiska belastningen konservativt med en faktor på 2 till 6,5 beroende på ram och analystyp. Denna konservatism orsakas av antaganden i Eurokod och i den tvådimensionella modellen.

Detta examensarbetet fann att om momentfördelningen tas hänsyn till vid beräkning av utnyttjandegraden med avseende på stabilitet enligt Eurokod kommer det att resultera i mindre konservativa beräkningar. För ramen utan voter liknade utnyttjandegraden den som härleddes från den olinjära statistiska analysen som utfördes på den tredimensionella modellen. För ramen med voter måste bidraget till stabiliteten från voterna implementeras i dimensioneringsverktyget för att få mer exakta resultat.

De styva kopplingarna mellan balkar och takåsar modellerades för att undersöka om den ökade rotationsstyvheten, för de punkter där takåsarna var fästa vid balkarna, skulle hjälpa till att stabilisera ramen. Denna studie fann att modellering av kopplingarna som de är idag inte kommer att bidra till ökad stabilitet. Om kopplingarna mellan takåsar och balkar förbättrades från enbultsförband till tvåbultsförband skulle det vara av intresse att implementera detta i dimensioneringsverktyget.

Acknowledgements

This master's thesis has been made in collaboration between the Division of Structural Mechanics at LTH and FS Dynamics.

First of all, we would like to thank our supervisors Prof. Kent Persson at the Division of Structural Mechanics at LTH, and Martin Eriksson and Mikael Fredenberg at FS Dynamics for their guidance throughout our work.

We would also like to thank Johan Jeppsson and Henry Eriksson at FS Dynamics and Joakim Truedsson at Altair for technical assistance regarding the design tool and the finite element program Hyperworks.

We would also like to express our gratitude to the fifth floor at V-building and the Lund office of FS Dynamics for hosting us. A special thanks to FS Dynamics for inviting us to their annual ski trip to Åre and several AWs.

Lastly, a thank you to our families and friends for the moral support.



Melanie Deshayes

Lund, June 2024



Truls Solli Larsson

Lund, June 2024

Contents

Abstract	I
Sammanfattning	III
Acknowledgements	V
Table of Contents	VIII
1 Introduction	1
1.1 Background	1
1.1.1 The steel industry and carbon emissions	1
1.1.2 The history of collapsing hall buildings in Sweden	1
1.1.3 Pre-existing design tool	2
1.2 Aim and objective	2
1.3 Method	3
1.4 Limitations	3
2 Theory	5
2.1 Steel as a building material	5
2.1.1 Material properties	5
2.1.2 Connections and joints	6
2.2 Instability in structural components	7
2.2.1 Flexural buckling of compressed components	7
2.2.2 Lateral torsional buckling of bending components	8
2.2.3 Eurocode and stability requirements	10
2.3 Finite element method	12
2.3.1 Linear static one-dimensional system	12
2.3.2 Three-dimensional finite element formulation	13
2.3.3 Non-linear model	15
2.3.4 Element types	17
2.3.5 Eigenvectors and eigenvalues	18
3 Models	21
3.1 Two-dimensional model	21
3.1.1 Subdivision and implementation of haunches	21
3.1.2 Boundary- and load conditions	22
3.1.3 Material model	23
3.2 Three-dimensional model	23
3.2.1 Method	23
3.2.2 Geometry	24

3.2.3	Material model	24
3.2.4	Boundary conditions	25
3.2.5	Load conditions	27
3.2.6	Mesh convergence study	31
4	Comparison of the models	35
4.1	Linear static analysis	35
4.1.1	Reaction forces	36
4.1.2	Normal force and moment diagram	37
4.1.3	Deflection	39
5	Critical load and utilization	43
5.1	Linear buckling analysis	43
5.2	Non-linear static analysis	45
5.3	Comparison with the two-dimensional model	51
6	Improvements to existing model	53
6.1	Considering moment distribution in stability analysis	53
6.2	Rigid connections between beam and purlins	57
7	Discussion	63
7.1	Comparison between the two models	63
7.2	Critical load	64
7.3	Utilization in stability analyses	64
7.4	Modelling of rigid connections between beam and purlins	65
8	Conclusions	67
9	Further studies	69
	Bibliography	71
A		73
A.1	Effects of different boundary conditions	73
A.2	Fixed boundary condition	75

1 Introduction

1.1 Background

Future stricter requirements on global greenhouse gas emissions from the steel and iron industry along with the history of collapsing hall buildings in Sweden laid ground for the incentive to investigate a design tool for steel frames used in hall buildings. These steel frames are shown in Fig. 1.1.

1.1.1 The steel industry and carbon emissions

The steel and iron industry stands for approximately 7-9% of the global greenhouse gas emission and therefore has a big influence on meeting the requirements of a more sustainable future [1]. The increased demand for a sustainable use of steel in combination with the International Energy Agency (IEA), stating that the steel demand will increase by 25-30% by the year 2050, puts even more pressure on mindful use of the material. One method to take both these requirements into account is to optimize the dimensions of building components. By mindfully calculating and optimizing the design and dimensions according to given requirement, will lead to less material use. Reducing the use of material will result in less greenhouse emission [2].

1.1.2 The history of collapsing hall buildings in Sweden

During the winter of 2009-2010 around 180 hall buildings in Sweden collapsed due to heavy snow fall [3]. During that winter the snow fall was heavy but did not exceed the specific snow load on the ground according to the European standards. The calculation of snow load according to Eurocode is based on reports from the Swedish Meteorological and Hydrological Institute (SMHI). This meant that the snow was not the main issue but highlighted other concerns in the structures. The collapses were mainly due to design errors and execution on site [3]. The buildings that were most prone to collapse were larger buildings with large spans, low angled roofs and built within the last 30 years. The main technical flaw was the lack of lateral stability. Another contributing factor that led to collapse were unsymmetrical snow load on the roof of the buildings. This meant heavy snow load on the leeward side and low snow load in the windward side on roofs with an angle lower than 15°. The building material were mainly steel and timber, only one case of a damaged concrete structure was reported [4].



Figure 1.1: Construction of steel frames used in a hall building. Taken from <https://www.lr-system.se/stalhallar/>.

1.1.3 Pre-existing design tool

A program for designing steel frames will be examined in the master's thesis. It is used for evaluating specific frames or to generate an optimized frame from the requirements given by the user. All the calculations are done according to Eurocode and the program can handle permanent loads, as dead weight, and variable load, as snow load and wind load. The stability of the frame is also calculated according to stability formulas in Eurocode, here the user can choose to add or not to add lateral stabilizing supports along the frame.

The program also allows the user to add haunches, struts, additional openings, equipment loads and storage loads. Furthermore, beam-profiles of types HEA and IPE are used for the frames that can be designed. These can also be combined in terms of beam and column depending on the users wishes. This design tool is programmed using the coding language Python and beam elements are used in a two-dimensional space. This type of element are thought to be sufficient for the calculations while remaining a low computational time.

1.2 Aim and objective

The aim of this thesis is to provide insight on how to increase the accuracy of simplified models when designing steel frames that use a minimum amount of material while maintaining the requirements given by the European standards for designing buildings. First, the design tool will be investigated to establish if the choice of element is proper for the kind of calculations needed. Secondly, the method for determining the material utilization for the frame will be investigated to establish if it is conservative or not. If the design tool is deemed to be too conservative, improvements will be suggested to reach a higher utilization.

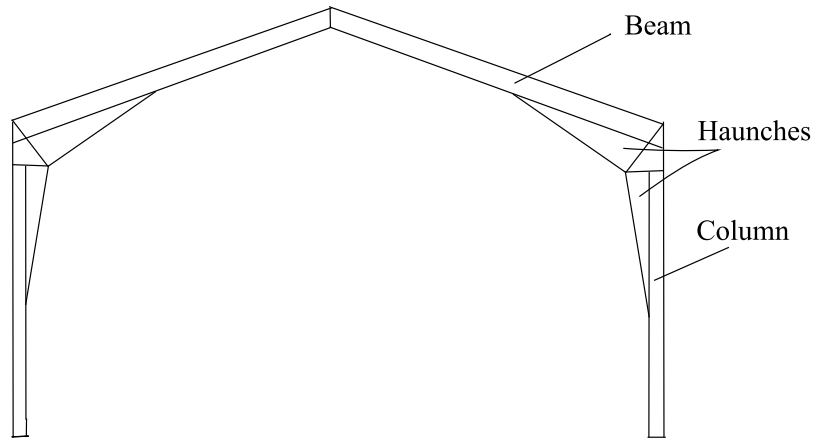


Figure 1.2: Illustration of a typical frame with haunches.

1.3 Method

Two different three-dimensional models using another kind of element, shell elements, were created using the finite element program HyperWorks. One frame with haunch and one without. An illustration of one of the frames can be seen in Fig. 1.2. A linear static analysis, a linear buckling analysis and a non-linear static analysis were performed. These analysis were used to determine if the choice of element are sufficient for calculations, if the method for calculating the utilization is correct and if the design tool is conservative or not. Lastly some improvements to the model were implemented and tested on the modelled three-dimensional frames.

1.4 Limitations

In the existing design tool, the option to add mid-supports at the gable frames is given to the user. These are added to add openings such as doors, windows or other openings. These mid-supports will not be investigated in this master's thesis. Openings can also be added in the length direction of the building, which will contribute to a varying distance between the frames. All hall buildings that will be investigated and compared will have the same centre distance between the frames.

Furthermore, a point load that represents equipment loads can be added by the user. This can be mounted on the inside of the walls or roof of the frames. These loads will neither be considered in this study. A storage load can also be added. This load occurs if the hall building is used as storage for granular material such as grain and soil. This will not be examined. In the design tool the connection to the ground can be chosen as fixed or pinned, but the only boundary condition considered in the three-dimensional models will be pinned. The design tool also considers every load case and load combination but the three-dimensional models consider one load case and one load combination that was deemed to be the most unfavourable in terms of applied load and utilization. Only the characteristic loads were used in the load combination for the snow load and dead weight. The wind load was multiplied with a reducing factor of 0.3.

2 Theory

2.1 Steel as a building material

For a long time, steel has been a fundamental building material due to its great material characteristics [5]. Especially for buildings with larger spans and a desire to minimize the material use. Steel has high compressive strength and almost equally high strength in tension, even when not combined with other materials. This makes it an independent building material. Something to be mindful of is that steel can be prone to corrosion and thermal deformation, thus must be protected from oxygen and high temperatures.

2.1.1 Material properties

When choosing steel as a construction material the essential characteristics are compressive and tensile strength, ductile behaviour and welding possibility [6]. Different steel types are often represented by stress-strain curves. In Fig. 2.1 a typical stress-strain curve for steel can be seen.

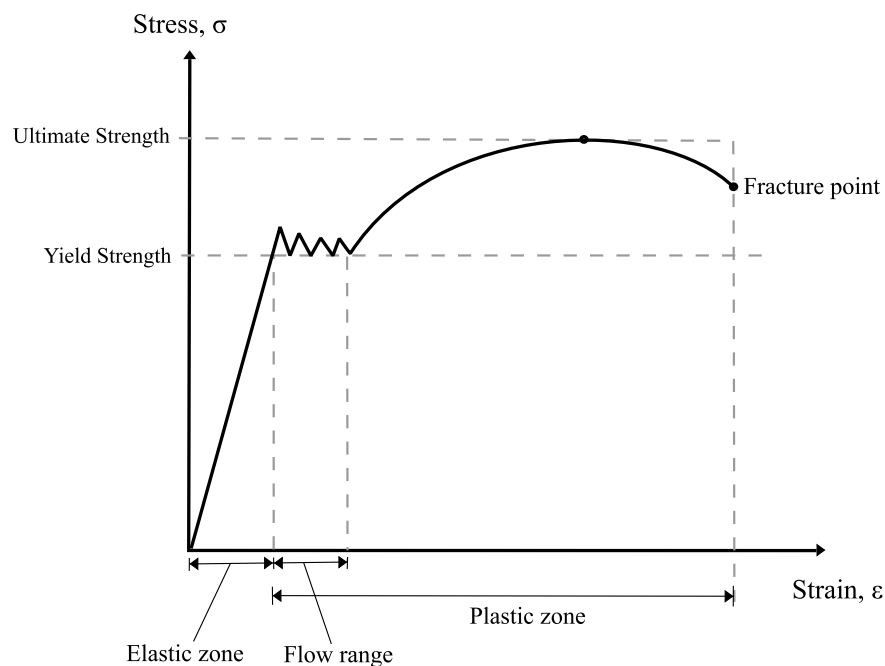


Figure 2.1: The relation between stress and strain in steel. Recreated from [7].

In Fig. 2.1 the relation between stress and strain are shown for construction steel being exposed to uniaxial tension. The different points marked in the figure show the most important parameters. The most interesting values are the strength of the steel, the modulus of elasticity and the shear modulus. The strength can be determined first by the yielding point, and then by the breaking point. When steel reaches the yielding point the material behaviour changes from elastic to plastic. Elastic behaviour is characterized by deformation that is reversible and plastic behaviour by deformation that is irreversible. The value of the yielding point is often used in capacity calculation for steel structures. A ductile behaviour of the steel material is requested when used as a building material because the maximum strength is reached after the yielding point, due to hardening effects, but also because the failure is not abrupt.

Furthermore, from the curve in Fig. 2.1, the modulus of elasticity can be calculated. This is the relation between the stress and strain in the elastic region for the material. The shear modulus cannot be determined only by the curve itself but can be calculated according to Eq. (2.1).

$$G = \frac{E}{2 \cdot (1 + \nu)} \quad (2.1)$$

where the modulus of elasticity is denoted E and the Poisson's ratio is denoted ν and is often chosen to be 0.3. Poisson's ratio is a factor that describes the ratio of transverse contraction strain to longitudinal extension strain in the direction of the stretching force.

2.1.2 Connections and joints

Different methods are used for connecting steel components and these are divided into mechanical connections and welded connections. The components can be beams and columns or flanges and webs. A bolted and a welded connection is illustrated in Fig. 2.2.

Bolted connections are a mechanical connection and are typically made of plates and

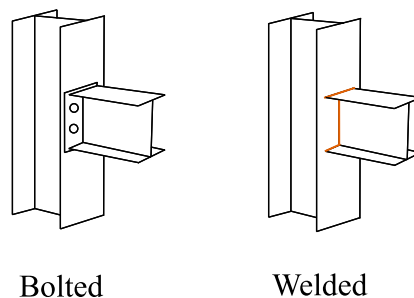


Figure 2.2: Example of different types of connections. Recreated from [8].

some sort of bolts that attach the two structural components together. The advantages are that these are easy to assemble on site and allow some movement in the joint, which is often advantageous regarding thermal expansion. Joints made with bolted connections, are considered as either pinned or as rigid in analysis, although the behaviour is semi-rigid in real practice. Pins are another mechanical connection and are used when the connected parts require free rotation. The connection is resembled as a hinge and only forces and no moments are transferred through this type of connection [8]. Welded connections often involves melting methods with high temperatures and electrode's that help with the fusion after solidification. They are more complex to execute therefore must be made in a controlled environment and by someone with the right expertise. The benefit of welds is the heightening of strength of the construction, durability and making the connection more rigid. One thing to be aware of when using welds is the possibility of fatigue failure and shrinkage of the welds [8].

2.2 Instability in structural components

Beyond making sure the material of the structure does not yield, the stability of a whole structure is of interest. There are several critical loads corresponding to different instability modes that need to be investigated and made sure the structure is secured against. Following the methods presented in Eurocode SS-EN 1993-1-1 the needs for stability will be met.

2.2.1 Flexural buckling of compressed components

Given that the axial force has no eccentricity, the component is straight, and the material has an elastic behaviour a critical buckling load for a structural component can be determined. The instability mode corresponding with this buckling load is flexural buckling and is shown in Fig. 2.3 [8].

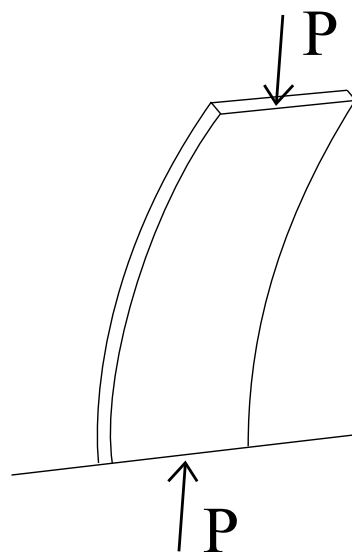


Figure 2.3: Conceptual illustration of flexural buckling. Recreated from [9].

By solving the differential equation in Eq. (2.2), where the displacement normal to the axial force is denoted w , the critical buckling load can be determined and is shown to Eq. (2.3)

$$EI \cdot w'''' + N \cdot w'' = 0 \quad (2.2)$$

$$N_{cr} = i^2 \frac{\pi^2 EI}{l_{cr}^2} \quad (2.3)$$

where the buckling mode is denoted i and the buckling length is denoted l_{cr} . A load that can produce multiple states of equilibrium is called a bifurcation load [9] and the first buckling mode has the corresponding bifurcation or buckling load according to Eq. (2.4). The first three buckling modes are illustrated for a simply supported beam in Fig. 2.4.

$$N_{cr} = \frac{\pi^2 EI}{l_{cr}^2} \quad (2.4)$$

When compressed in the axial direction, thin open cross-sections can experience torsional or torsional-flexural buckling. The component twists around its shear center and does not deflect. The corresponding instability mode for this critical load is torsional flexural buckling and is shown in Fig 2.5 [8].

2.2.2 Lateral torsional buckling of bending components

Beams subjected to bending can displace in the weak axis direction, v , according to Fig. 2.6 [8]. The bending causes compression in one part of the cross-section and tension in the other. The lateral displacements v for the two flanges differs in a state of equilibrium in a deformed position. Destabilizing forces in the same direction as the displacement are acting on the flange that is subjected to compression and stabilizing forces in the opposite direction of the displacements on the flange in tension. Because of this the displacements in the compressed flange grow faster and as a result the cross section is twisting. This instability mode, where the component is subjected to both lateral displacements and torsion, is called lateral torsion buckling [8] and can be seen in Fig. 2.6.

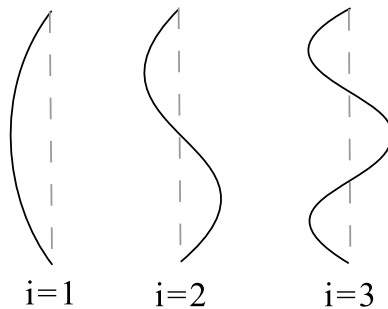


Figure 2.4: The first three buckling modes for a simply supported beam. Recreated from [9].

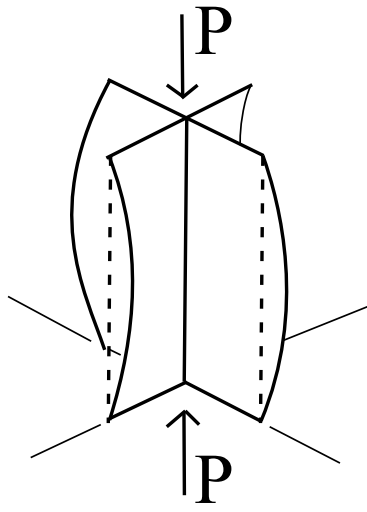


Figure 2.5: Conceptual illustration of torsional-flexural buckling. Recreated from [9].

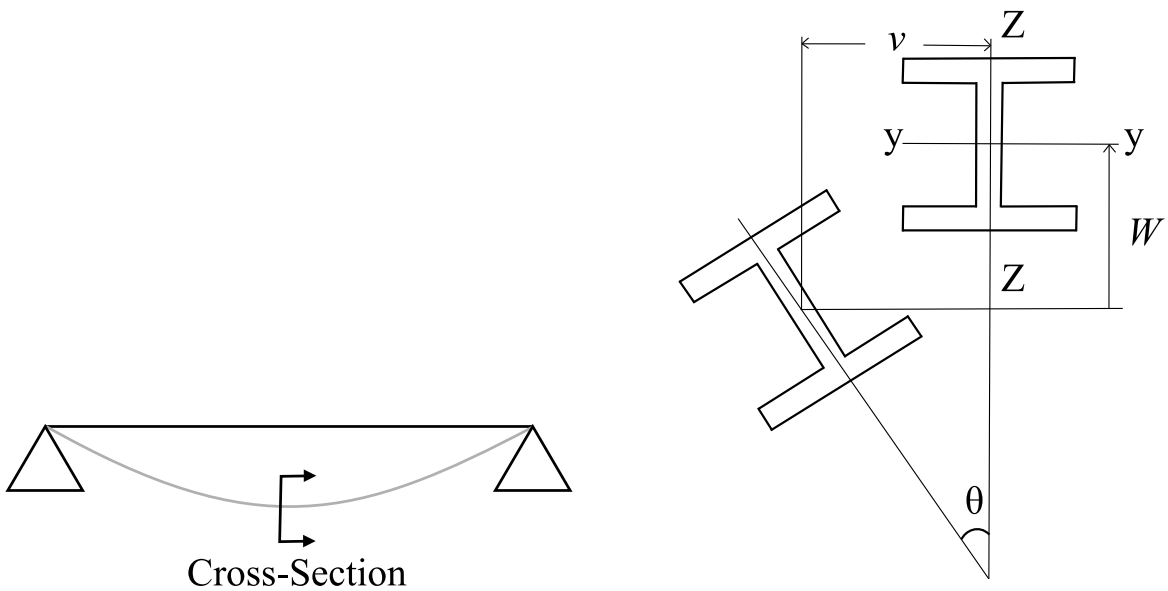


Figure 2.6: A simply supported beam subjected to later torsional buckling and its cross-section. Recreated from [9].

2.2.3 Eurocode and stability requirements

In Eurocode SS-EN 1993-1-1 2005 there is a procedure for determining the utilization of structural components in regards to stability with the requirement that it is below one. These requirements are described in this chapter.

Structural components in compression

When designing a structural component subjected to compression, instability should be taken into consideration with the requirement that the relation between the design force and force capacity is below one [10]. This relation can be expressed as shown in Eq. (2.5).

$$\frac{N_{Ed}}{N_{b,Rd}} \leq 1 \quad (2.5)$$

where the design compressive force and force capacity regarding instability are denoted N_{Ed} and $N_{b,Rd}$ respectively. When calculating the force capacity, the class of the cross-section needs to be taken into consideration where the regular area is chosen for class 1-3 and effective area is chosen for class 4. The calculations for force capacity are shown in Eqs. (2.6) and (2.7).

$$N_{b,Rd} = \frac{\chi A f_y}{\gamma_{M1}} \quad (2.6)$$

$$N_{b,Rd} = \frac{\chi A_{eff} f_y}{\gamma_{M1}} \quad (2.7)$$

where the reduction factor for relevant instability mode is denoted χ , the cross-section area and effective area are denoted A and A_{eff} , the yield strength of the material is denoted f_y and the partial coefficient γ_{M1} takes capacity regarding instability into consideration. The reduction factor χ , shown in Eq. (2.8), is determined by buckling curve and should not be higher than one [10]

$$\chi = \frac{1}{\phi + \sqrt{\phi^2 - \bar{\lambda}^2}} \leq 1 \quad (2.8)$$

where

$$\phi = 0.5[1 + \alpha(\bar{\lambda} - 0.2) + \bar{\lambda}^2] \quad (2.9)$$

and the slenderness parameter $\bar{\lambda}$ is calculated with two different methods depending on the class of cross-section, the difference being identical to the method for calculating force capacity. The calculation for the slenderness parameter is shown in Eqs. (2.10) and (2.11)

$$\bar{\lambda} = \sqrt{\frac{A f_y}{N_{cr}}} \quad (2.10)$$

$$\bar{\lambda} = \sqrt{\frac{A_{eff} f_y}{N_{cr}}} \quad (2.11)$$

where the imperfection factor is denoted α and the elastic critical normal force for relevant instability mode based on the gross cross-section is denoted N_{cr} .

Structural components in bending

When designing a structural component un-braced in the lateral direction being subjected to bending around the stiff axis, the effects of lateral torsion buckling should be taken into consideration [10]. The relation between designing acting bending moment and bending capacity must be below one. This is shown in Eq. (2.12)

$$\frac{M_{Ed}}{M_{b,Rd}} \leq 1 \quad (2.12)$$

where the designing acting bending moment and bending moment capacity regarding instability are denoted M_{Ed} and $M_{b,Rd}$ respectively. Calculating the bending moment capacity using Eq. (2.13)

$$M_{b,Rd} = \chi_{LT} W_y \frac{f_y}{\lambda_{M1}} \quad (2.13)$$

where the bending resistance is denoted W_y . The bending resistance is determined depending on the class of cross-section. For class 1-2 a plastic bending resistance is chosen whereas for class 3 and 4 an elastic and an effective bending resistance is chosen respectively. The reduction factor for lateral-torsion buckling is denoted χ_{LT} and is calculated in a similar way as for the reduction factor for buckling and must not exceed one. The calculation is shown in Eqs. (2.14) and (2.16)

$$\chi_{LT} = \frac{1}{\phi_{LT} + \sqrt{\phi_{LT}^2 - \bar{\lambda}_{LT}^2}} \leq 1, 0 \quad (2.14)$$

where

$$\phi_{LT} = 0.5[1 + \alpha_{LT}(\bar{\lambda}_{LT} - 0.2) + \bar{\lambda}_{LT}^2] \quad (2.15)$$

$$\bar{\lambda}_{LT} = \sqrt{\frac{W_y f_y}{M_{cr}}} \quad (2.16)$$

where the imperfection factor is denoted α_{LT} . The slenderness parameter for lateral torsion buckling is denoted $\bar{\lambda}_{LT}$ and the elastic critical moment for lateral torsion buckling is denoted M_{cr} . The elastic critical moment for lateral torsion buckling takes loading conditions, real moment distribution and lateral restraints into consideration.

Structural components in bending and compression

If an analysis with second order effects including imperfections is disregarded the following stability analysis should be made for double symmetric cross-sections, which the beam-profiles of IPE and HEA both are [10]. Structural components subjected to bending and compression simultaneously that are un-braced for torsion and are prone to twist must satisfy the following criteria shown in Eqs. (2.17) and (2.18).

$$\frac{N_{Ed}}{\frac{\chi_y N_{Rk}}{\gamma_{M1}}} + k_{yy} \frac{M_{y,Ed} + \Delta M_{y,Ed}}{\frac{\chi_{LT} M_{y,Rk}}{\gamma_{M1}}} + k_{yz} \frac{M_{z,Ed} + \Delta M_{z,Ed}}{\frac{\chi_{LT} M_{z,Rk}}{\gamma_{M1}}} \leq 1,0 \quad (2.17)$$

$$\frac{N_{Ed}}{\frac{\chi_z N_{Rk}}{\gamma_{M1}}} + k_{zy} \frac{M_{y,Ed} + \Delta M_{y,Ed}}{\frac{\chi_{LT} M_{y,Rk}}{\gamma_{M1}}} + k_{zz} \frac{M_{z,Ed} + \Delta M_{z,Ed}}{\frac{\chi_{LT} M_{z,Rk}}{\gamma_{M1}}} \leq 1,0 \quad (2.18)$$

Depending on the cross-section class, the interaction factors denoted k_{yy} , k_{yz} , k_{zy} and k_{zz} are determined. The additions in moment caused by a displacement of the center of gravity are denoted ΔM_{Ed} and $\Delta M_{z,Ed}$.

2.3 Finite element method

The finite element method is a numerical method used in structural mechanics when the behaviour of complex structures is of interest [11]. The structure is divided into small finite elements, each possessing an approximation of the displacement over the element. The variation of the unknown variable, which for structural mechanics typically are displacements and rotations, is described with shape functions. This method allows for complex behaviour to be described with simple approximations reaching a more accurate depiction of the real behaviour with smaller elements. The smaller the elements, the greater the computational cost. Therefore, it is important to achieve a balance where the computational cost is not too high while still achieving an accurate result, when modelling using the finite element method.

2.3.1 Linear static one-dimensional system

In a static one-dimensional system, a relation between displacements and external forces is expressed. The stiffness of the body determines the deformation corresponding to the applied force. A simple system can be described with a spring example, two nodes with one degree of freedom each connected by a spring with a stiffness, see Fig. 2.7 and Eq. (2.19).

$$\begin{bmatrix} k & -k \\ -k & k \end{bmatrix} \begin{bmatrix} u_1 \\ u_2 \end{bmatrix} = \begin{bmatrix} f_1 \\ f_2 \end{bmatrix} \quad (2.19)$$

$$\mathbf{k}_e \quad \mathbf{u} = \mathbf{f}$$

where the element stiffness matrix is denoted \mathbf{k}_e , the displacement vector is denoted \mathbf{u} and the external force vector is denoted \mathbf{f} . Knowing the boundary condition for one

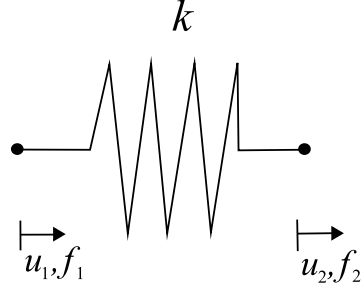


Figure 2.7: A simple two-node spring element.

node and the force applied to the other node, the system has two unknown variables and with two equations the system can be solved. With several elements a global stiffness matrix is assembled, from each element stiffness matrix, and a global system can be expressed in Eq. (2.20)

$$\mathbf{K} \mathbf{u} = \mathbf{f} \quad (2.20)$$

where the global stiffness matrix is denoted \mathbf{K} . Displacement vector and force vector \mathbf{u} and \mathbf{f} contains displacements and external forces for every node, respectively. Using the finite element method for solving a static linear problem means solving this system.

2.3.2 Three-dimensional finite element formulation

A four-node element in a three-dimensional space with six degrees of freedom in each node, three for translation in x -, y - and z -direction and three for rotation around these three axis. The global system will consist of a stiffness matrix with 24 rows and 24 columns, a displacement vector with 24 rows and one column and an external force vector with 24 rows and one column. To determine the stiffness matrix \mathbf{K} a differential equation describing the equilibrium between the internal and external forces acting on a body must be solved [11]. The differential equation is solved by approximating the displacement variation within each element using shape functions. The equilibrium equation for three-dimensional elastic problem is written as shown in Eq. (2.21)

$$\tilde{\nabla}^T \sigma + \mathbf{b} = 0 \quad (2.21)$$

where the gradient matrix for the stresses is denoted $\tilde{\nabla}^T$, the stress vector is denoted σ and the body forces are contained in vector \mathbf{b} . The stress vector and body force vector include forces in all directions. Including traction forces \mathbf{t} acting on the surface of the body, multiplying the expression with an arbitrary weight function \mathbf{v} , integrating over the region and rewriting the equation by partial integration the weak form is gathered, see Eq. (2.22).

$$\int_V (\tilde{\nabla} \mathbf{v})^T \sigma dV = \int_S \mathbf{v}^T \mathbf{t} dS + \int_V \mathbf{v}^T \mathbf{b} dV \quad (2.22)$$

To derive the three-dimensional finite element formulation a shape function matrix \mathbf{N}

is used to approximate the variation of displacements over each element. With this method the displacements \mathbf{u} can be expressed according to Eqs. (2.23-2.27)

$$\mathbf{u} = \mathbf{N} \mathbf{a} \quad (2.23)$$

and using Galerkin's method the arbitrary weight function \mathbf{v} can be expressed as

$$\mathbf{v} = \mathbf{N} \cdot \mathbf{c} \quad (2.24)$$

When \mathbf{v} and \mathbf{c} are arbitrary constants [11] the gradient can be written as

$$\tilde{\nabla} \mathbf{v} = \mathbf{B} \cdot \mathbf{c} \quad (2.25)$$

where \mathbf{B} can be written as

$$\mathbf{B} = \tilde{\nabla} \mathbf{N} \quad (2.26)$$

Taking this into consideration the weak form is rewritten to

$$\int_V \mathbf{B}^T \sigma dV = \int_S \mathbf{N}^T \mathbf{t} dS + \int_V \mathbf{N}^T \mathbf{b} dV \quad (2.27)$$

The constitutive model for an elastic material is written as shown below in Eq. (2.28)

$$\sigma = \mathbf{D} \epsilon \quad (2.28)$$

This equation is inserted into the weak form where the constitutive matrix is denoted \mathbf{D} . The strain is the gradient of the displacements according to kinematic relations making the constitutive model as shown in Eq. (2.29)

$$\sigma = \mathbf{D} \mathbf{B} \mathbf{a} \quad (2.29)$$

Making the distinction of different boundary conditions where either the traction vector \mathbf{t} or the displacement vector \mathbf{u} is prescribed, natural and essential boundary condition respectively, the finite element formulation is expressed as Eq. (2.30) .

$$\begin{aligned} \left(\int_V \mathbf{B}^T \mathbf{D} \mathbf{B} dV \right) \mathbf{a} &= \int_{S_h} \mathbf{N}^T \mathbf{h} dS + \int_{S_E} \mathbf{N}^T \mathbf{t} dS + \int_V \mathbf{N}^T \mathbf{b} dV \\ \mathbf{K} \mathbf{a} &= \mathbf{f}_b + \mathbf{f}_l \end{aligned} \quad (2.30)$$

where

$$\mathbf{t} = \mathbf{S} \mathbf{n} = \mathbf{h} \text{ on } S_h \quad (2.31)$$

$$\mathbf{u} = \mathbf{g} \text{ on } S_g \quad (2.32)$$

2.3.3 Non-linear model

In a non-linear finite element model, both the geometry and material can have a non-linear behaviour. To solve a finite element equation using a non-linear model a different method is used and plasticity of the material can be included.

Non-linear geometry

In a non-linear model the contributions from geometrical non-linearity is taken into consideration, if the displacements are large enough [12]. The stiffness of the structure changes with the displacement of the structure therefor every load step in the Newton-Raphson scheme, the tangent stiffness \mathbf{K}_t is calculated using the Total Lagrangian formulation according to Eq. (2.33)

$$\mathbf{K}_t = \mathbf{K}_0 + \mathbf{K}_\sigma + \mathbf{K}_u \quad (2.33)$$

where the initial linear stiffness is denoted \mathbf{K}_0 . The additional stiffness matrices arise from internal forces and displacements denoted \mathbf{K}_σ and \mathbf{K}_u respectively.

Plasticity and von Mises criterion

A yield criterion is established to model plasticity in the material model to determine when the material starts yielding. To model plasticity in steel the von Mises criterion is commonly used [13] and this yield criterion is shown in Eq. (2.34)

$$\sqrt{3J_2} - \sigma_{y0} = 0 \quad (2.34)$$

where

$$\begin{aligned} \sqrt{3J_2} = & \left[\frac{1}{2} [(\sigma_{11} - \sigma_{22})^2 + (\sigma_{22} - \sigma_{33})^2 + (\sigma_{33} - \sigma_{11})^2] \right. \\ & \left. + \frac{1}{3} (\sigma_{12}^2 + \sigma_{23}^2 + \sigma_{13}^2) \right]^{1/2} \end{aligned} \quad (2.35)$$

and the initial yield stress in pure tension is denoted σ_{y0} .

Solution of a non-linear equilibrium equation

When solving Eq. (2.20) using a non-linear model the stiffness matrix \mathbf{K} changes with the displaced geometry of the structure [13]. The solution to Eq. (2.20) is therefor divided into increments of steps. The Newton-Raphson iteration scheme solves Eq. (2.36)

$$\mathbf{K}_t(\mathbf{a}^i - \mathbf{a}^{i-1}) = \mathbf{f}_{n+1} - \mathbf{f}_{int} \quad (2.36)$$

where the current displacement for iteration i is denoted \mathbf{a}^i and the displacement for previous iteration is denoted \mathbf{a}^{i-1} . The known load is denoted \mathbf{f}_{n+1} and the internal forces from previous iteration is denoted \mathbf{f}_{int} . The tangent stiffness is denoted \mathbf{K}_t which describes the stiffness of the structure with the current displaced geometry.

By controlling the equilibrium between external and internal forces, using the Newton-Raphson algorithm, Eq. (2.36) can be solved [13]. This is done with an iterative procedure adjusting the displacements until near equilibrium is achieved. For every load step a new load is applied and the iterative process is performed again. Tangent stiffness, \mathbf{K}_t , is determined, current displacement, \mathbf{a}^i , is solved, strains, stresses and internal forces are calculated. Next load step can initiated with new displacements, strains, stresses and internal forces. This is illustrated in Fig. 2.8.

Close to a peak load, or critical load, the Newton-Raphson scheme does not converge [13] and this is illustrated in Fig. 2.9. If the determinant of \mathbf{K}_t is equal to zero, the equation system shown in Eq. (2.37) possesses a non-trivial solution. This implies difficulties using this scheme.

$$\mathbf{K}_t \dot{\mathbf{a}} = 0 \quad (2.37)$$

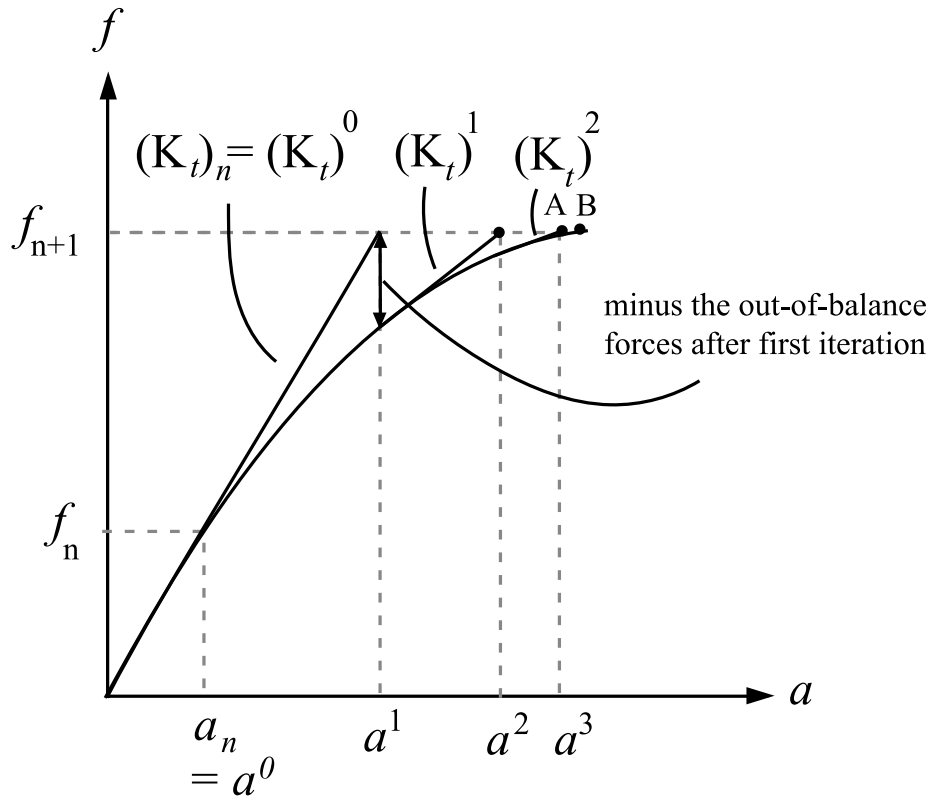


Figure 2.8: The Newton-Raphson iteration.

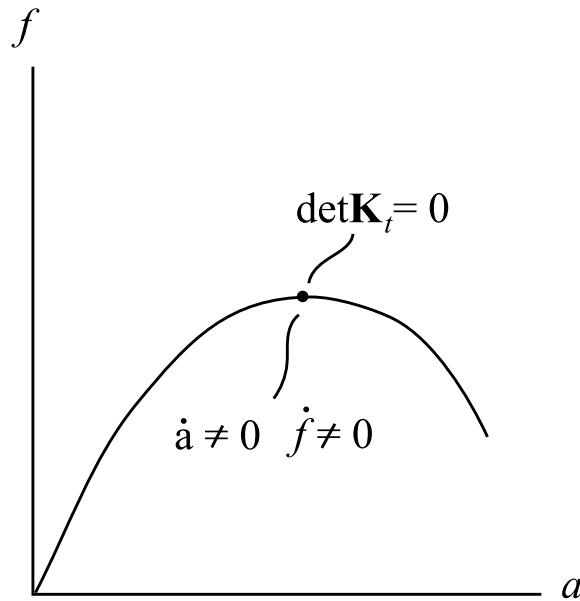


Figure 2.9: Newton-Raphson scheme does not converge close to peak.

2.3.4 Element types

The design tool and the finite element software, HyperWorks, uses the finite element method to calculate the behaviour of the steel frame. Two different approaches were used as one is in a two-dimensional space and the other in a three-dimensional space. Beam elements were used in the design tool and shell elements were used in HyperWorks when creating the three-dimensional model of the frame.

Beam element

Beam elements incorporates the effects of axial deformation a bar is prone to when subjected to loading and shear and rotational deformation a beam is prone to when subjected to loading [9]. In a two-dimensional space a beam element therefor has six degrees of freedom, three for each node see Fig. 2.10. Structural components where the height of the cross-section is larger compared to the width and thickness are sufficiently modelled with beam elements to reduce computational cost. This approximation is possible as the prominent stresses are in the longitudinal direction. Through this method normal forces, shear forces and bending moments can be extracted to use in further analysis of a structure.

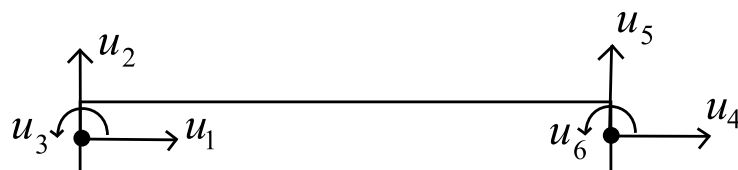


Figure 2.10: A beam element and its degrees of freedom.

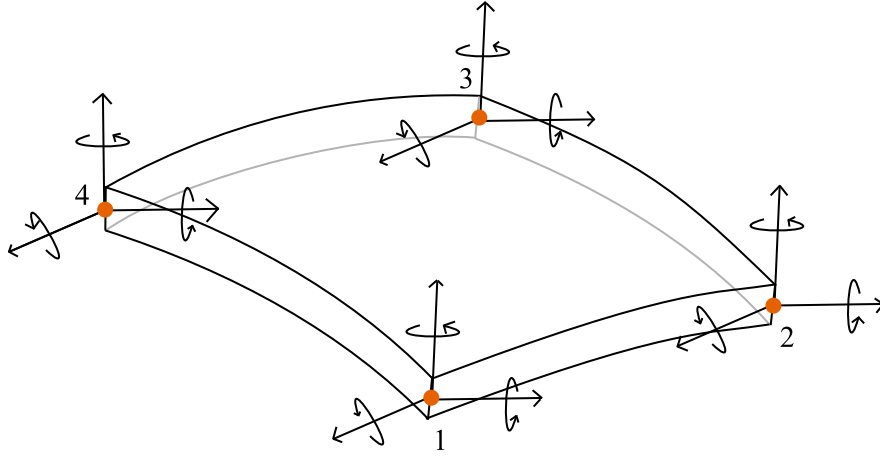


Figure 2.11: A shell element and its degrees of freedom.

Shell element

Structural components with a thickness that is small compared to the length and width are best modelled using shell elements. Stresses in the normal direction of a shell element are neglected. A conventional four-node shell element has translation and rotational degrees of freedom in all directions for each node, see Fig. 2.11.

2.3.5 Eigenvectors and eigenvalues

With the help of eigenvectors and eigenvalues, critical loads can be predicted. When running a linear buckling analysis in a finite element solver, the results are eigenvalues that can be multiplied with the initial applied load. The pure definition of the eigenvalue problem is stated in Eq. (2.38) where $F(x)$ is a linear function, \mathbf{A} is a quadratic matrix, also called a transformation matrix, $\bar{\mathbf{x}} \neq \mathbf{0}$ is the eigenvector and λ is the eigenvalue [14].

$$F(x) = \mathbf{A}\bar{\mathbf{x}} = \lambda\bar{\mathbf{x}} \quad (2.38)$$

The definition states that if a vector $\bar{\mathbf{x}}$ is mapped on to the function $F(x)$ they have to be parallel for $\bar{\mathbf{x}}$ to be defined as a eigenvector. Thus making the value λ the eigenvalue. This value can be a scalar of any sort, negative or positive. To calculate the eigenvalue, Eq. (2.38) can be rearranged as shown in Eqs. (2.39 - 2.41), where Eq. (2.40) is the well-known eigenvalue problem and Eq. (2.41) is called the characteristic equation.

$$\lambda\bar{\mathbf{x}} - \mathbf{A}\bar{\mathbf{x}} = 0 \quad (2.39)$$

$$(\lambda\mathbf{I} - \mathbf{A})\bar{\mathbf{x}} = 0 \quad (2.40)$$

$$\det(\lambda\mathbf{I} - \mathbf{A}) = 0 \quad (2.41)$$

When solving the eigenvalue problem, the eigenvector indicates the displacements and the eigenvalues are the scale factors that can be applied to the eigenvectors. There are as many eigenvalues for a model as there are degrees of freedom.

3 Models

3.1 Two-dimensional model

The existing design tool uses a two-dimensional model based on beam elements to calculate section forces, stresses and displacements. All calculations and designing are performed with algorithms implemented using the programming language Python.

3.1.1 Subdivision and implementation of haunches

The frame is divided into ten parts, two for each column and three for each beam, which is then divided into several elements. The standard value is set to ten elements per part and is used for this comparison, shown in Fig. 3.1. The subdivision is used to enable the modelling of the frame where haunches are placed. The division is dependent of the length of the haunches. The elements used in the two-dimensional model are beam elements and with described subdivision the model consists of 100 elements, 101 nodes and 303 degrees of freedom.

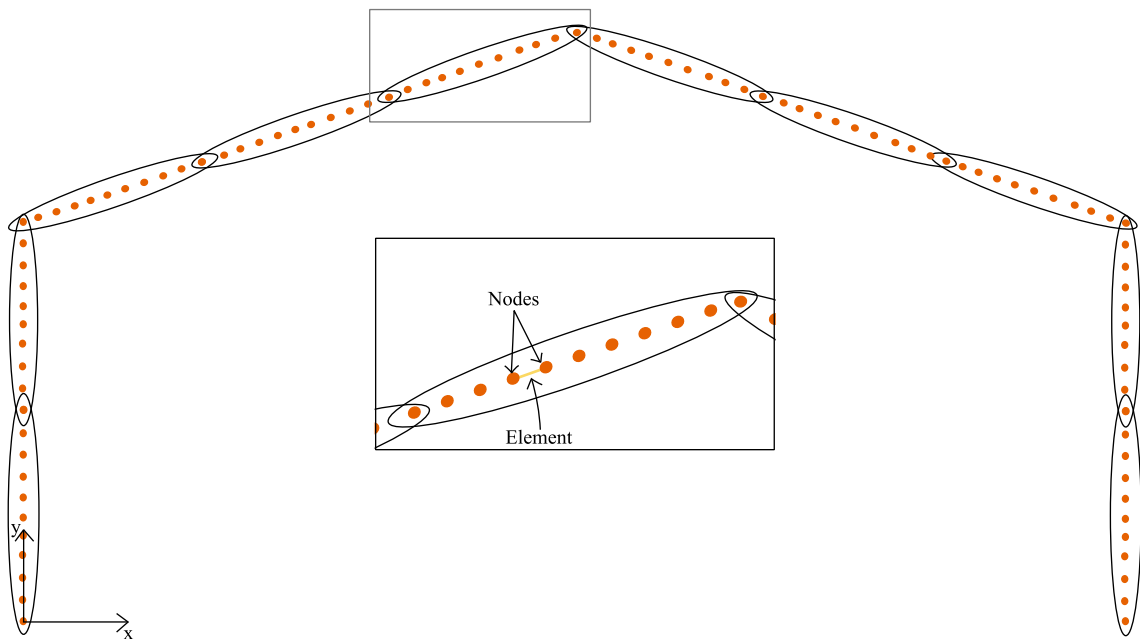


Figure 3.1: The subdivision of the model used in the design tool.

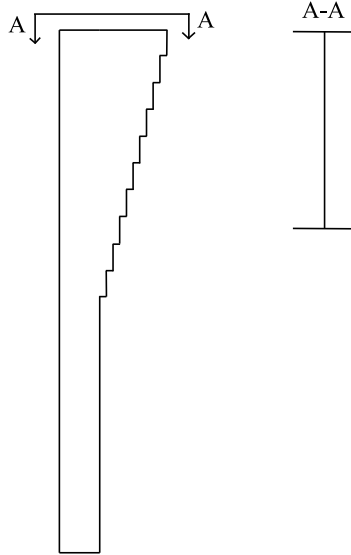


Figure 3.2: Visualization of how the haunch is implemented in the design tool along with the cross-section of the haunch at the top of the column.

The method for implementing haunches in the design tool is to create a larger cross-section for the part corresponding to the haunch. In reality the cross-section of the haunch changes linearly and in the two-dimensional model the ten elements cross-section changes step-wise following the haunch, shown in Fig. 3.2. The haunches contribution to the stability of the frame is neglected when calculating the utilization in regards to stability according to Eurocode. This is a conservative approach and the contribution is neglected by not including the cross-sectional area for the haunch when performing the calculations.

3.1.2 Boundary- and load conditions

A pinned boundary condition is used for the beam-to-ground connection by setting the displacement to zero for first, second, 301st and 302nd degree of freedom. These degrees of freedom represent the translation in horizontal and vertical direction for the first and last element closest to the ground. The displacement vector for the system is shown in Eq. (3.1).

$$a = \begin{bmatrix} 0 \\ 0 \\ a_3 \\ \vdots \\ a_{300} \\ 0 \\ 0 \\ a_{303} \end{bmatrix} \quad (3.1)$$

The loads are calculated according to Eurocode and consists of permanent load, as dead weight of the frame, och variable loads, as wind and snow load. More on how these loads are calculated can be found in section 3.2.5.

3.1.3 Material model

The design tool only considers linear and elastic material behaviour. The material used is steel S355, which means the steel will yield at 355 MPa. The modulus of elasticity and Poisson's ratio was chosen to 210 GPa and 0.3, respectively.

3.2 Three-dimensional model

In this chapter, a description of the modelling of two different steel frames is presented. The intention is to choose two frames that varied in cross-section, span and the inclusion of haunches or not. The first frame that was chosen had the beam-profile of IPE240, for both the columns and beams, and with haunches. The second frame had the beam-profile of IPE360, for both the columns and beams, without haunches. These two frames were chosen due to the span being quite similar and therefore difference of the haunches and cross-section would be highlighted.

3.2.1 Method

HyperWorks, a finite element program, was used to create a three-dimensional model of the two frames. First, the geometry of the model was created from existing blue prints, to ensure the geometry of the frame was based in reality. When the geometry of the frame was established a mesh of shell elements was applied. Then the chosen boundary conditions and relevant loads, calculated according to Eurocode, were applied. The same conditions were implemented in the design tool used for the two-dimensional model using beam elements.

When the model was established, a linear static analysis, a linear buckling analysis and a non-linear static analysis were performed using OptiStruct as the solver. From the linear static analysis the cross-section forces, deflections and stresses were obtained. Reaction forces, normal forces, moments and displacements were compared between the models to establish if the three-dimensional model was correctly constructed and that the two-dimensional model used a sufficient element type. The linear buckling analysis revealed what failure mode, regarding stability, was relevant and the corresponding critical buckling load. The critical buckling load was then compared with the two-dimensional model. The non-linear model used in this analysis include an ideal elasto-plastic material with von Mises yield criterion without hardening effects. The load is acting as a follower load and depend on the displacement of the frame changing direction from the initial direction each load step. The load was divided into twenty load-steps and the initial load-step was zero. This analysis also determined the critical failure load and this was compared to the critical failure load derived from the linear buckling analysis, but also the two-dimensional model.

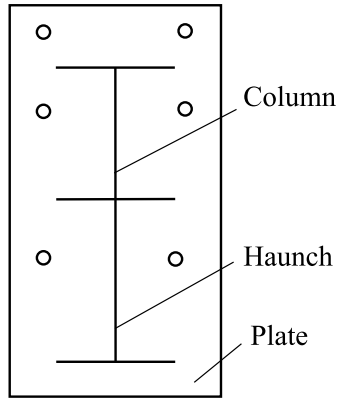


Figure 3.3: The cross-section of a corner of a frame with haunch.

3.2.2 Geometry

The frames consist of two columns and two beams. The beams make up the roof of the frame with a certain angle and are constrained to the columns at the corners of the frame. The beams and columns have beam-profiles of IPE and the cross-sections are therefore double symmetric. For the frames that need reinforcement in terms of haunches, these can be attached to the beam and the column. This changes the geometry of the corner of the frame and how the column-to-beam connection is made. This also changes the cross-section at the part where a haunch is attached, see Fig. 3.3 for a sketch of a reinforced cross-section.

At the bottom of the column the connection between the frame and the ground consists of a plate and two bolts. At the corner of the frames the column and beam are connected with two plates and bolts and the same connection is used at the top of the frame. This was modelled as one plate with double thickness as it was regarded as a rigid connection. In the three-dimensional model the density of all the plates were neglected. This is because the plates are not taken into consideration in the two-dimensional model and to make the initial comparison more accurate, the same conditions were applied in the three-dimensional model. This implies that the stiffness of the plate is included in the model but the dead load from the plates are not.

The first frame that was modelled had beam-profiles of IPE240 for both column and beam and had haunches in the corners. The second frame had beam-profiles of IPE360 and was without haunches. The frames are shown in Figs. 3.4 and 3.5 respectively.

3.2.3 Material model

The material used to model the frame was steel S355, which means that the steel will yield at 355 MPa. The modulus of elasticity and Poisson's ratio was chosen to 210 GPa and 0.3 respectively. The material model for the linear analysis was elastic and ideal elasto-plastic for the non-linear analysis.

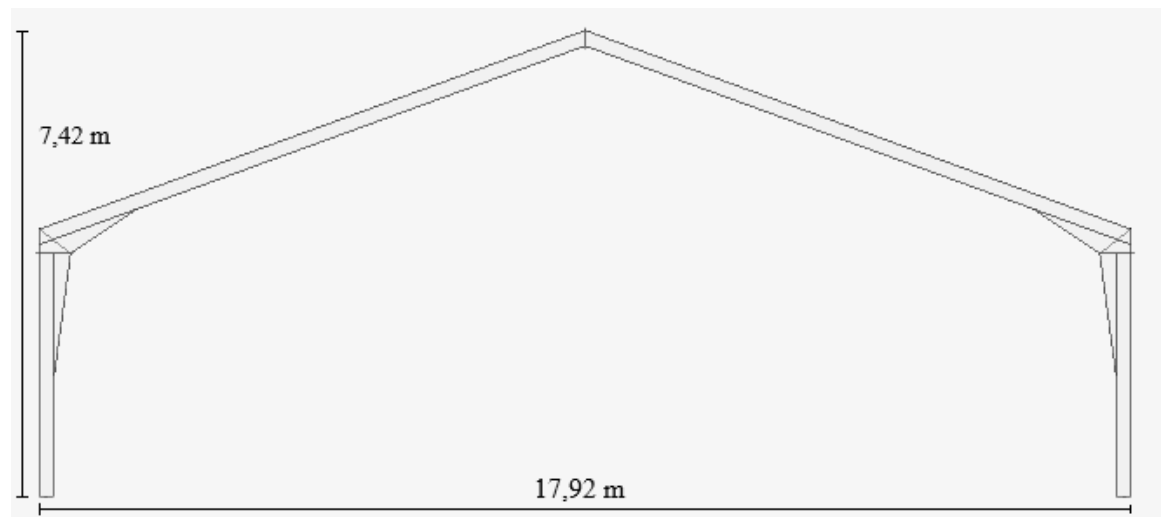


Figure 3.4: The geometry of the frame with beam-profiles IPE240 with haunches.

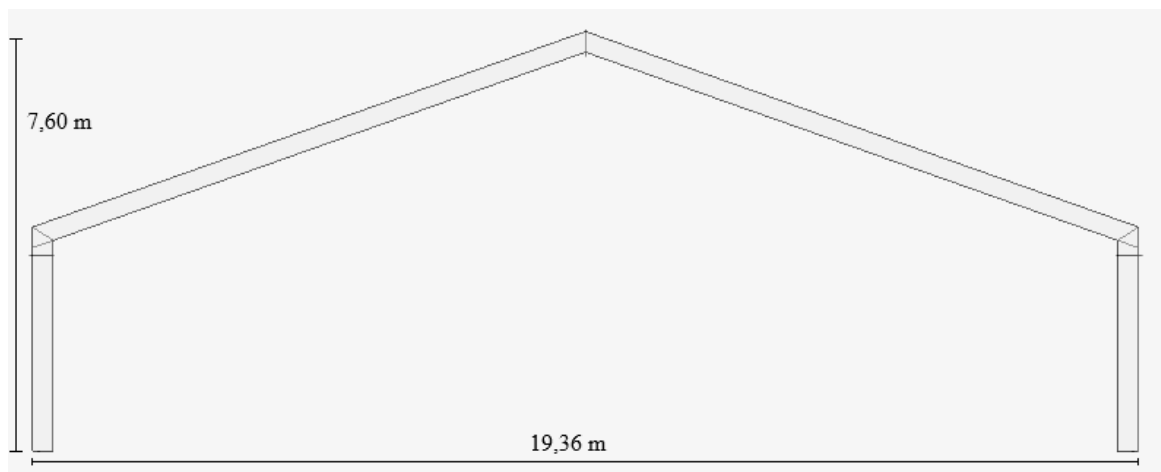


Figure 3.5: The geometry of the frame with beam-profiles IPE360 without haunches.

3.2.4 Boundary conditions

It is a pinned boundary condition, as in the design tool, that is to be replicated for the three-dimensional model. Three boundary conditions were investigated for the three-dimensional model and the one where reaction forces were best comparable to the reaction forces for the two-dimensional model was used. The two other boundary conditions are shown in Appendix A. The chosen boundary condition was to restrict translation in all directions around the holes, where the bolts are fastened, in the plate connecting to the ground. The boundary is visualized in Fig. 3.6. A pinned boundary condition is possible due to rigid connections at the corners and at the top of the frame, where thick plates are placed, which create stability.

To model the frames connection to the rest of the hall building, restraints for the frame to move in and out of the plane were assigned along the whole frame. The constrains was placed along the outer flange in the middle and restraining the frame from moving out of the plane along the outer flange as shown in Fig. 3.7. This was seen as a good approximation as the distances between the purlins that connects the frame to the

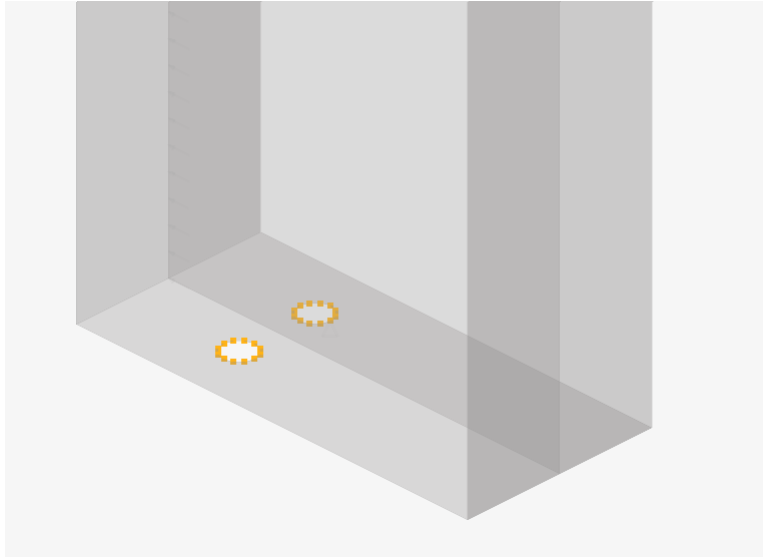


Figure 3.6: Clarification of the chosen boundary condition where all translations are restrained around the highlighted area.

rest of the hall building are small. The distances for the frames with beam-profiles of IPE240 and IPE360 are 1000 mm and 800 mm, respectively. This accounts for ten and 13 purlins for each beam for respective frame.

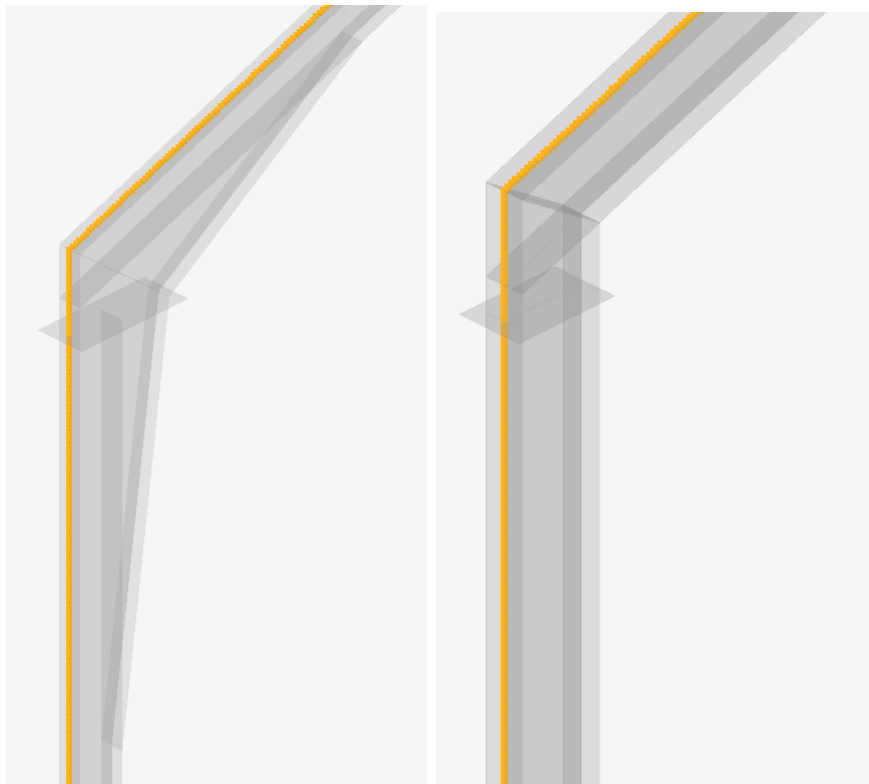


Figure 3.7: The constraint restraining the frame from moving in and out of plane.

3.2.5 Load conditions

The loads that were applied to both models were calculated according to Eurocode. This included permanent load, wind load and snow load. The worst load combination was used in the analysis as seen in Fig. 3.8. The wind load was reduced by a factor of 0.3 whereas the permanent and snow loads have no reducing factor. An imperfection load of 1 kN was applied on the frame when executing the non-linear static analysis. This load was applied in the out-of-plane direction on the bottom flange in the middle of the right beam, see Fig. 3.9. This imperfection load was included to create an imperfection of geometry to achieve instability as the other loads are applied in the plane.

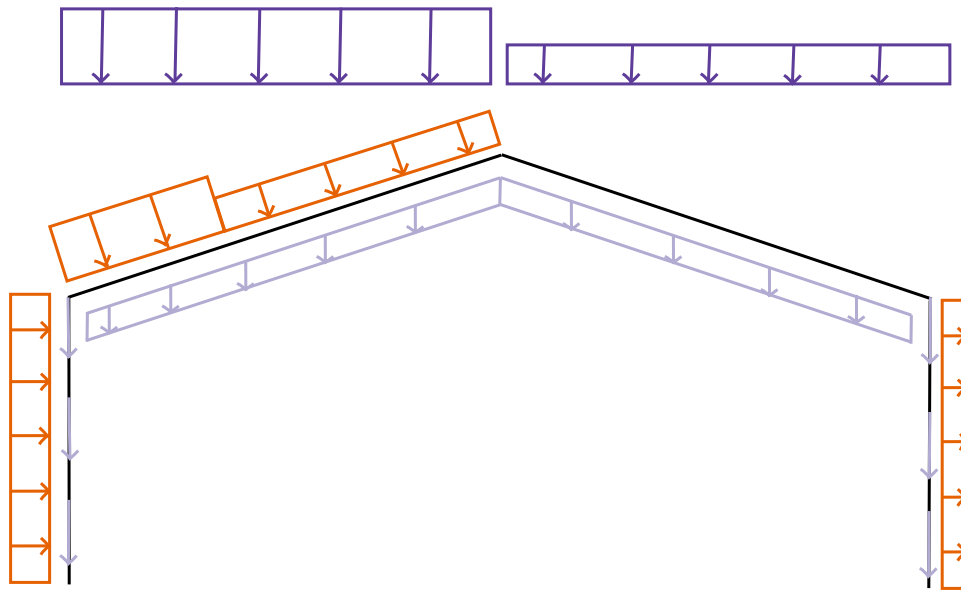


Figure 3.8: Load combination used in the analysis. The light purple loads are the permanent loads, the purple loads are the snow load and the orange loads are the wind loads.

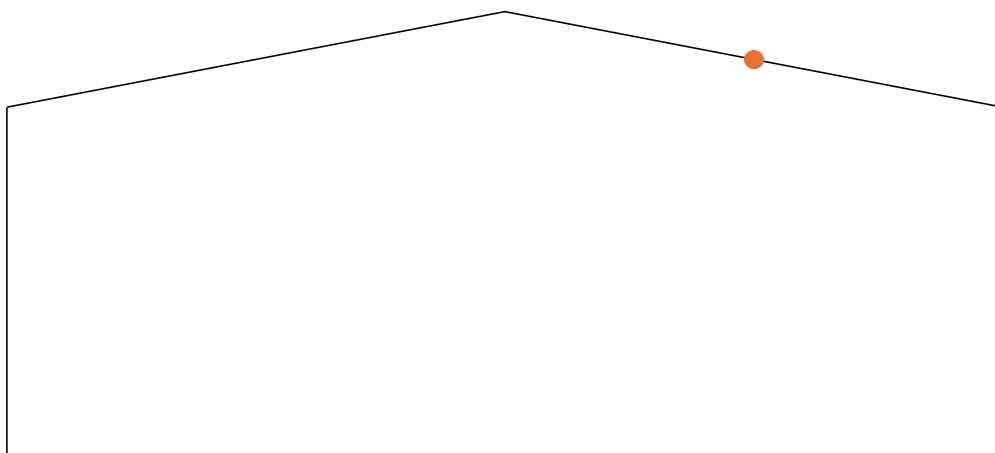


Figure 3.9: Illustration of the placement of the imperfection load.

Permanent load

The permanent load consists of dead weight of the columns, beams, ribs and purlins. The dead weight was implemented in HyperWorks with the GRAV function, which automatically calculates the weight of the structure and is added as a load. The weight of the ribs and purlins were implemented as a distributed load where the value of the weight was taken from the design tool for simplicity.

Wind load

When calculating the acting wind load on the frame the procedure in SS-EN 1991-1-4 2005 was followed. The wind load is varying along the height of the frame but conservatively the highest load is applied over the whole region, which is in compliance with the design tool. Depending on the angle of the roof the load has a pressure or suction effect on the frame. If it has a suction effect on the roof in load combination with snow load, the worst case is to apply a load with zero force [15]. Only the external wind load was calculated since the two-dimensional model did not consider internal wind load. The equation for external wind load is shown in Eq. (3.2)

$$w_e = q_p(z_e)c_{pe} \quad (3.2)$$

where the form factor for external wind load is denoted c_{pe} , the characteristic reference wind pressure $q_p(z_e)$ and the reference height z_e . The characteristic wind pressure was calculated with knowledge of exposure and wind speed both determined by the surrounding terrain. This is shown in Eq. (3.3)

$$q_p(z) = [1 + 6 \cdot I_v(z)] \cdot \left[k_r \cdot \ln \left(\frac{z}{z_0} \right) \cdot c_0(z) \right]^2 \cdot q_b \quad (3.3)$$

where the turbulence intensity at height z , $I_v(z)$, the terrain factor k_r and the reference wind pressure q_b is calculated using Eqs. (3.4-3.6) [15]

$$I_v(z) = \frac{1}{c_0(z) \cdot \ln \left(\frac{z}{z_0} \right)} \quad (3.4)$$

$$k_r = 0,19 \cdot \left(\frac{z_0}{z_{0,II}} \right) \quad (3.5)$$

$$q_b = \frac{1}{2} \cdot \rho \cdot v_b^2 \quad (3.6)$$

where the minimum height for chosen terrain category is denoted z_{min} . The roughness length is denoted z_0 , the topography factor c_0 , the roughness length for terrain category 2 $z_{0,II}$, the density for air ρ and the reference wind speed denoted v_b . For a height z below the minimum height z_{min} gives $q_p(z) = q_p(z_{min})$

When choosing the form factors for the external wind, $c_{pe,10}$ was always chosen due to the area always exceeding 10 m^2 . For the columns, the form factor was chosen from

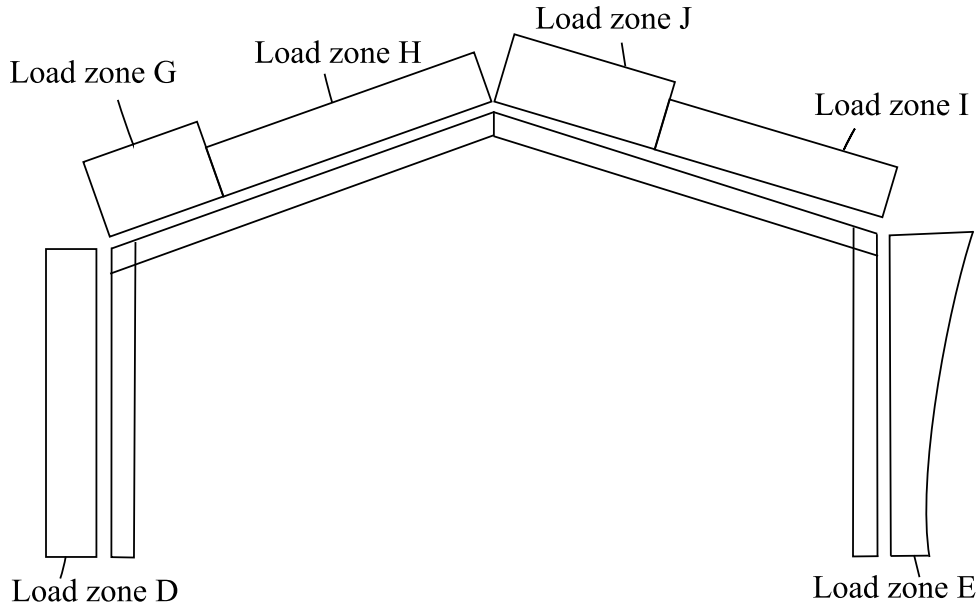


Figure 3.10: An illustration of the zones for the wind load acting on the frame.

the tables provided by SS-EN 1991-1-4 from chapter 7.2 [15]. The relation between the height of the column, h , and span of the building, d , was used for interpolation when needed. For the roof, the same table used for the columns were used together with the angle of the roof. When needed, interpolation was done to calculate the correct $c_{pe,10}$ value for the correct section. For gable roof the roof is divided into different zones. In this case a frame that would be placed in the middle of the hall structure was chosen, thus the roof will be divided into six zones, see Fig. 3.10.

When the form factors and characteristic reference wind pressure was calculated the characteristic external wind load could be calculated according to Eq.(3.2). The load in zones J and I was put set to zero as this was the worst load case scenario as previously stated.

Snow load

The characteristic snow load was determined by following Eurocode SS-EN 1991-1-3. It will act as a variable load and calculated using Eq. (3.7)

$$S = \mu_i C_e C_t s_k \quad (3.7)$$

where the characteristic snow load is denoted s_k and depends on the geographic location and the form factor based on the roof is denoted μ_i . The exposure factor is denoted C_e and determined by table 5.2 in SS-EN 1991-1-3 and the coefficient determining the energy losses through the roof is denoted C_t and is normally set to 1.0 [16]. Both frames have gable roofs thus the form factor varies between the right and left side and was determined from SS-EN 1991-1-3.

Overview of loads

The loads acting on the frames as described in Fig. 3.8 are presented as a short overview in table 3.1 and table 3.2 for frame with beam-profiles IPE240 and IPE360 respectively.

Table 3.1: Forces acting on frame with beam-profiles IPE240 with haunches.

Load	x -direction [kN]	y -direction [kN]
Permanent load acting on left column	-	1.54
Wind load acting on left column	3.96	-
Permanent load acting on left beam	-	8.76
Wind load acting on left beam	1.54	3.76
Snow load acting on left beam	-	57.28
Permanent load acting on right beam	-	8.76
Snow load acting on right column	-	42.96
Permanent load acting on right column	-	1.67
Wind load acting on right beam	1.40	-
Total load	6.90	124.73

Table 3.2: Forces acting on frame with beam-profiles IPE360 without haunches.

Load	x -direction [kN]	y -direction [kN]
Permanent load acting on left column	-	1.91
Wind load acting on left column	3.27	-
Permanent load acting on left beam	-	11.19
Wind load acting on left beam	1.35	3.99
Snow load acting on left beam	-	61.95
Permanent load acting on right beam	-	11.19
Snow load acting on right column	-	46.46
Permanent load acting on right column	-	1.91
Wind load acting on right beam	1.18	-
Total Load	5.80	138.60

3.2.6 Mesh convergence study

To determine what mesh size to use for following analyses, a mesh convergence study was performed. The purpose of this was to ensure that the mesh that later was used was fine enough to get accurate results while still maintaining a low computational time. The study was done by comparing the von Mises stresses for different mesh sizes, then calculating a relative error from the smallest mesh size applied. Only the snow load was applied on the frames for this study due to this being the largest and an asymmetrical load. For the stresses, a designated area was chosen and an average value of the stress within the area was calculated. The designated area was chosen to be at the top flange at the corner of both frames as seen in Fig. 3.11.

It was analyzed at which mesh size the error converges to almost zero, which was then chosen as mesh size for further analysis. The study was performed on both frames to investigate if the different geometries converged with the same mesh size. To see how this converged, the relative error was plotted against the number of elements in the model. The result of the mesh convergence study can be seen in Fig. 3.12 and Fig 3.13.

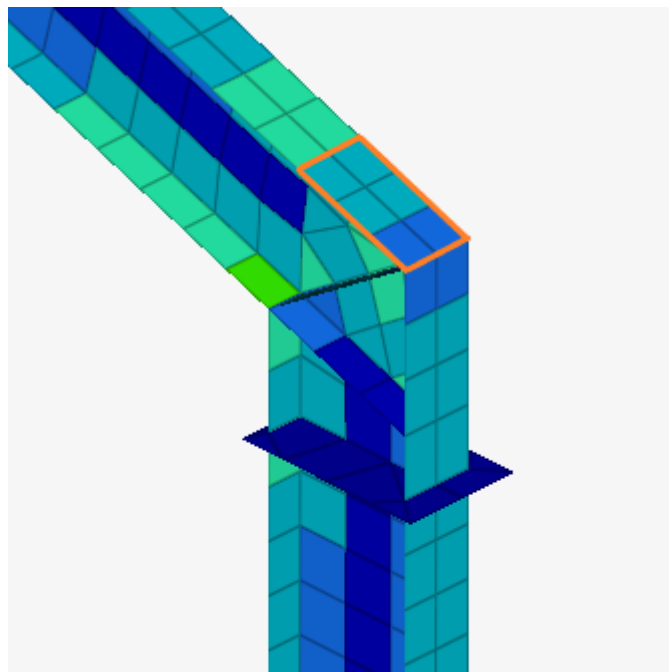


Figure 3.11: The area where the mean value of von Mises stresses were retrieved.

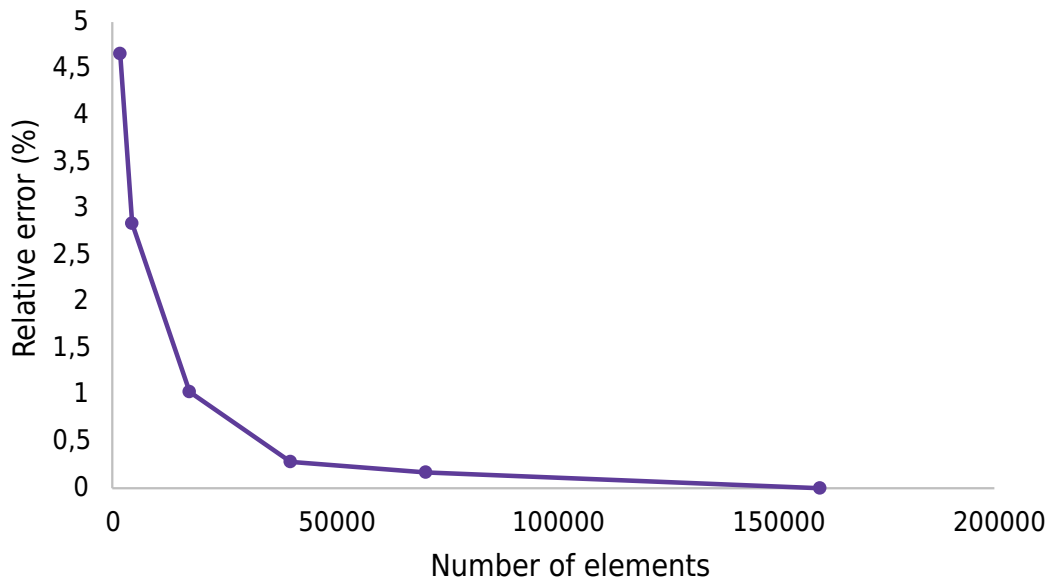


Figure 3.12: The result of a mesh convergence study for a frame with beam-profiles IPE240 with haunches.

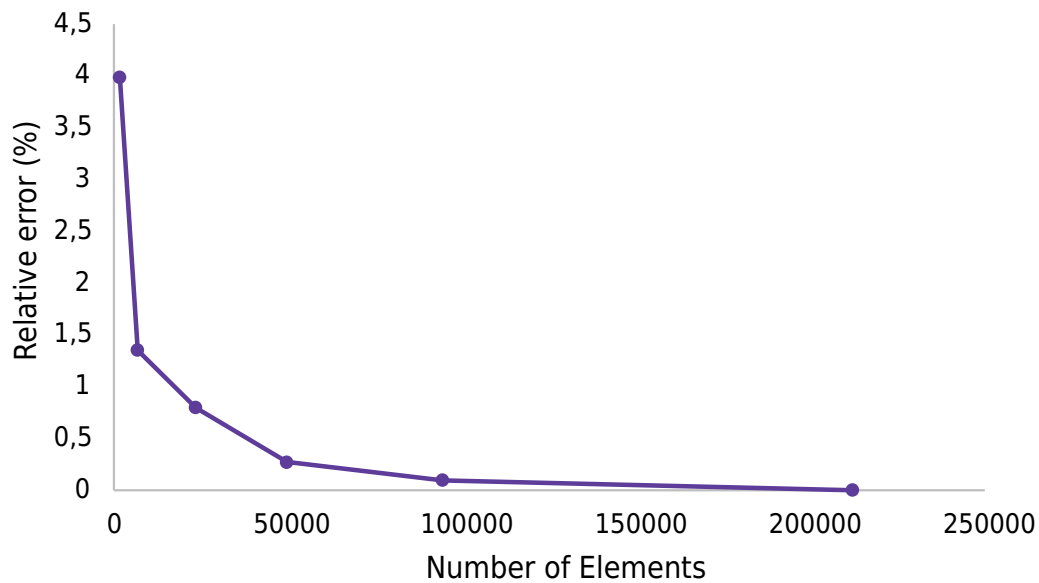


Figure 3.13: The result of a mesh convergence study for a frame with beam-profiles IPE360 without haunches.

The same mesh size, 20 mm, was used for both frames. This accounted for approximately 40300 and 49700 elements for the frame with beam-profile IPE240 and IPE360 respectively. The amount of elements was seen as sufficient as the relative error was below 0.5 % compared to the finest mesh size of 10 mm. See Fig 3.14 for some different mesh sizes visualized in the corners of both frames.

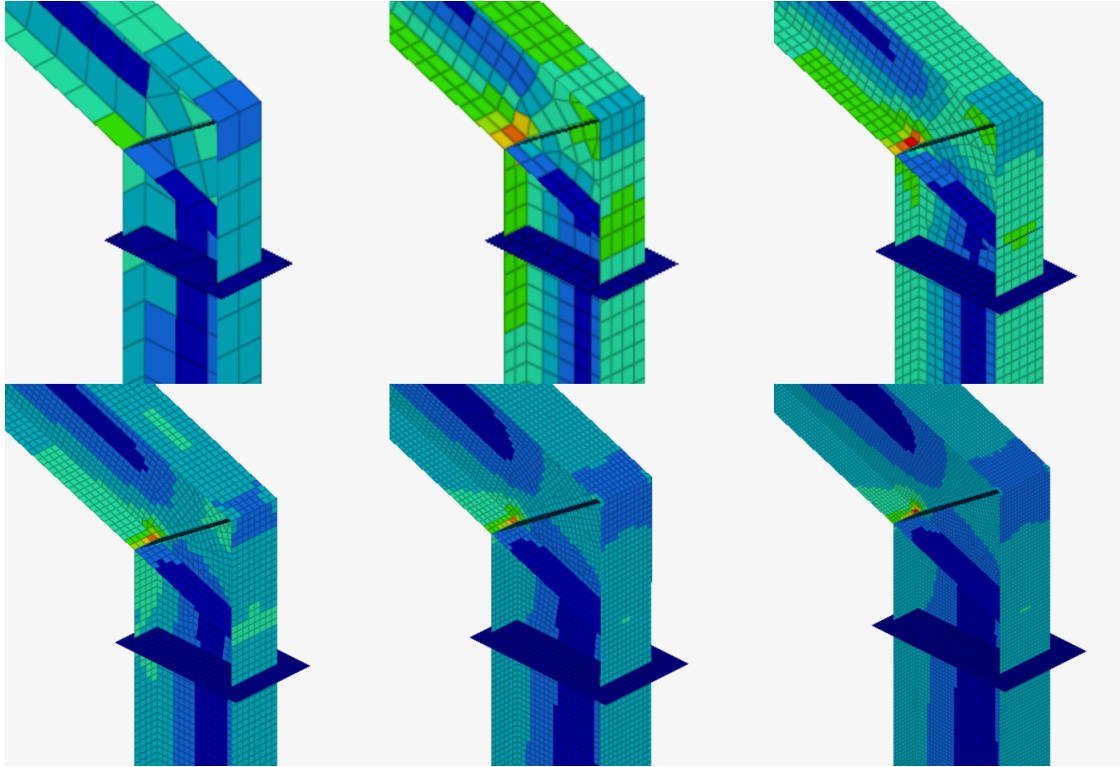


Figure 3.14: Visualization of a mesh-size of 120, 60, 30, 20, 15 and 10 mm. The chosen mesh-size was 20 mm.

4 Comparison of the models

A linear static analysis was performed on the three-dimensional model using shell elements to be able to compare cross-section forces and displacements with the two-dimensional model and to check that the two models produce comparable results for further comparisons. The fundamental conditions are applied load, material properties and geometry.

4.1 Linear static analysis

From the linear static analysis a visualization of the deformed frames, with a factor of 20, along with the stress distribution is presented in Figs. 4.1 and 4.2. The stress distribution for the right corner for both frames is presented in Fig. 4.3. The von Mises stresses for each element are shown, the legend bar shows the stress with a unit of MPa.

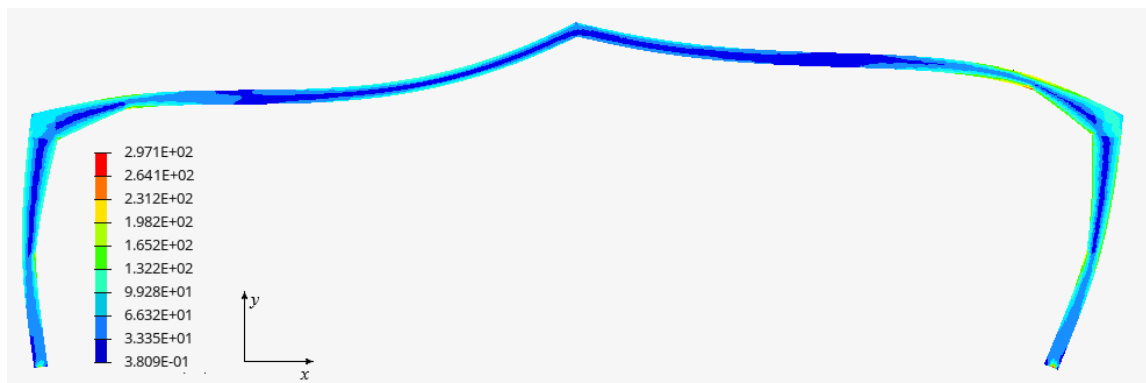


Figure 4.1: Deformed frame with beam-profiles IPE240 with haunches along with the stress distribution.

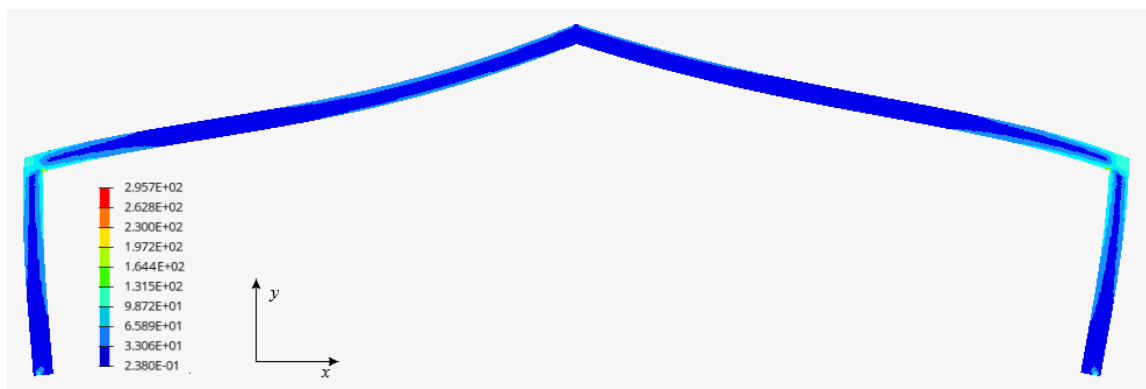


Figure 4.2: Deformed frame with beam-profiles IPE360 without haunches along with the stress distribution.

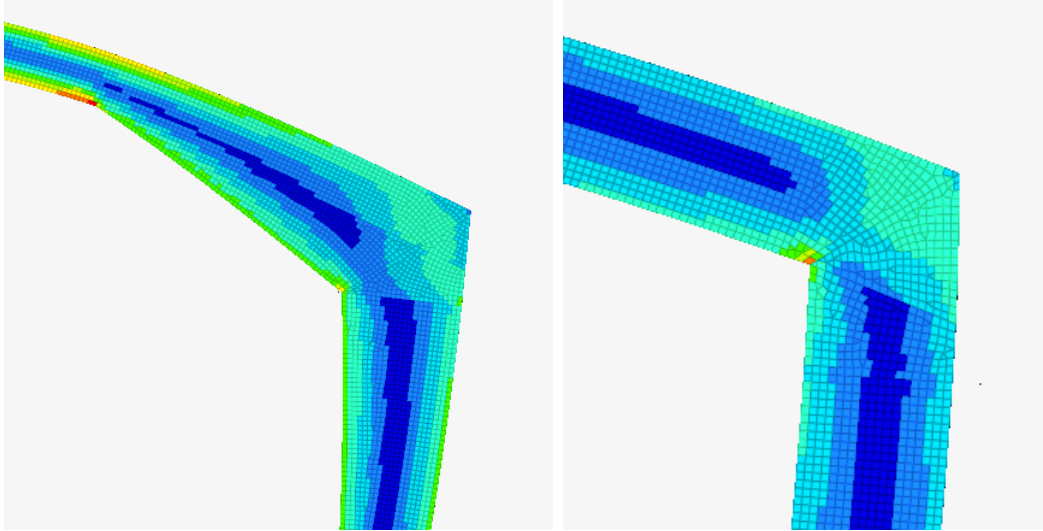


Figure 4.3: Deformed corners for both frames along with the stress distribution.

4.1.1 Reaction forces

To ensure that the applied load on the three-dimensional model was correct, the reaction forces for the frames were compared. The result of the different models and frames are presented in Tables 4.1 and 4.2. The reaction forces in the x - and y -direction are presented in these tables for both left and right supports, together with the difference in force and as a percentage.

Table 4.1: Reaction forces for models using shell and beam elements for a frame with beam-profiles IPE240 with haunches.

Left support	Shell Elements [kN]	Beam Elements [kN]	Diff. [kN]	Diff. [%]
x - direction	27.9	26.5	1.5	5.6
y - direction	65.9	64.2	1.7	2.6
Right support	Shell Elements [kN]	Beam Elements [kN]	Diff. [kN]	Diff. [%]
x - direction	-34.8	-32.5	-2.3	7.1
y - direction	58.8	57.5	1.2	2.1

Table 4.2: Reaction forces for models using shell and beam elements for a frame with beam-profiles IPE360 without haunches.

Left support	Shell Elements [kN]	Beam Elements [kN]	Diff. [kN]	Diff. [%]
x - direction	35.2	32.2	3.0	9.2
y - direction	73.6	71.5	2.2	3.0
Right support	Shell Elements [kN]	Beam Elements [kN]	Diff. [kN]	Diff. [%]
x - direction	-41.0	-37.7	-3.3	8.7
y - direction	65.0	63.9	1.1	1.7

4.1.2 Normal force and moment diagram

A further comparison of the two models was made, by comparing their normal-force-diagrams and moment-diagrams for the right beam of the frame. The right beam was chosen, as this structural component is of interest when investigating the failure modes analyzed in the linear buckling analysis, see section 5.1. The normal-force-diagrams are shown in Figs. 4.4 and 4.5.

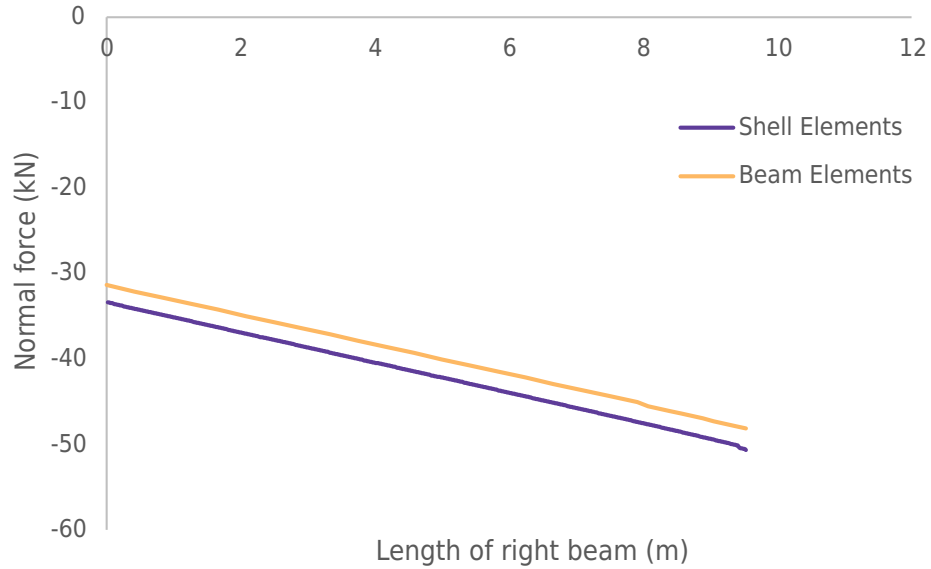


Figure 4.4: Normal force diagram of the right beam in a IPE240 frame with haunches. Normal force is represented by the vertical axis and the length of the right beam is represented by the horizontal axis

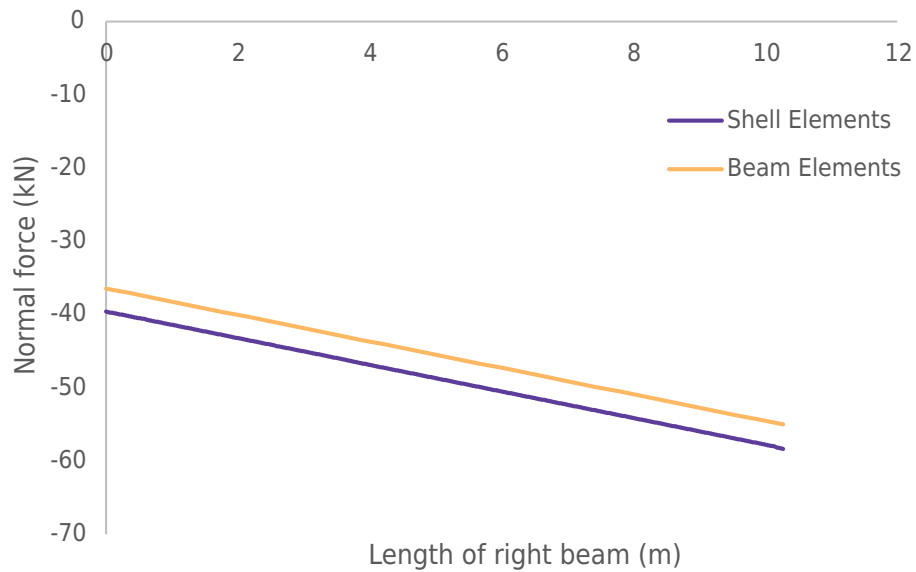


Figure 4.5: Normal force diagram of the right beam in a IPE360 frame without haunches. Normal force is represented by the vertical axis and the length of the right beam is represented by the horizontal axis.

As seen in the diagram the trend of the two lines are the same, but the value differs. The right beam is compressed more in the model using shell elements than the model using beam elements. To compare the moment distributions in the right beam the moment-diagrams are shown in Figs. 4.6 and 4.7. The moment distribution for the two-dimensional and three-dimensional model are similar and the same behaviour is seen in both models with different geometries.

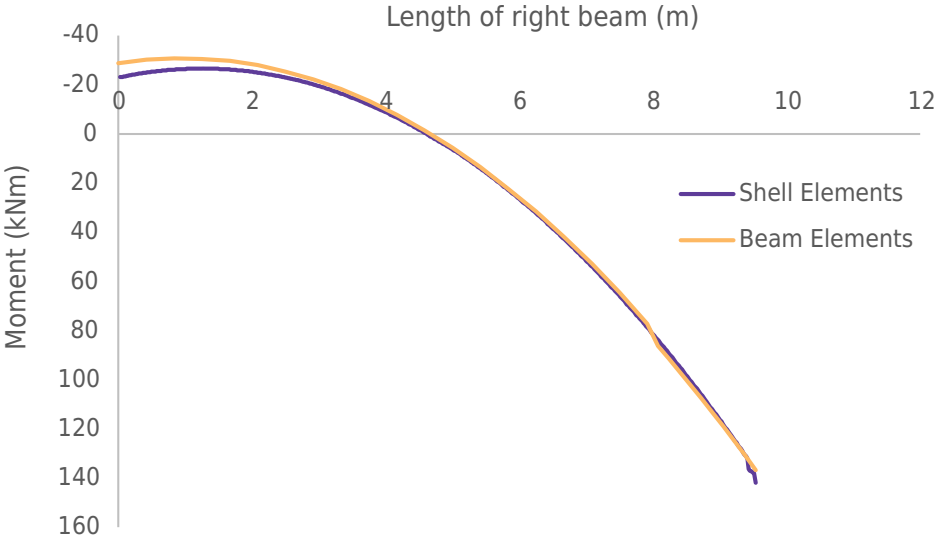


Figure 4.6: Moment diagram of the right beam in a IPE240 frame with haunches. The moment is represented by the vertical axis and the length of the right beam is represented by the horizontal axis.

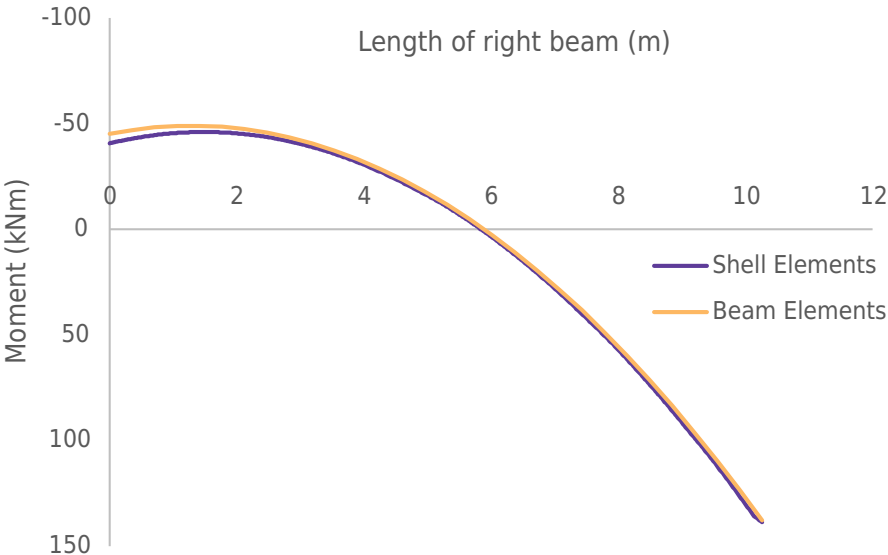


Figure 4.7: Moment diagram of the right beam in a IPE360 frame without haunches. The moment is represented by the vertical axis and the length of the right beam is represented by the horizontal axis.

4.1.3 Deflection

A comparison of the deflection of the frames were also made. The displacement from the three-dimensional model were extracted from the outer flange. The cross-section of the flange deforms minimally in a linear analysis, therefore it is a valid comparison with the two-dimensional model, where the displacements are extracted from the middle of the beam-profile. The comparison is presented in Figs. 4.8 and 4.9, where the height is represented by the vertical axis and the width of the frame is represented by the horizontal axis. In both figures the deflection has been multiplied with factor of 20 to enhance the differences.

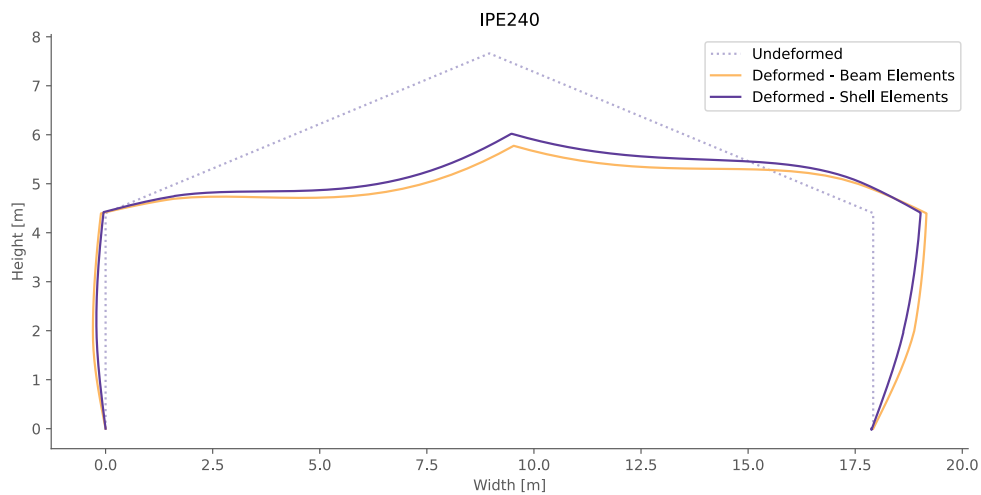


Figure 4.8: Displacement for the frame with beam-profiles IPE240 for both the two- and three dimensional model.

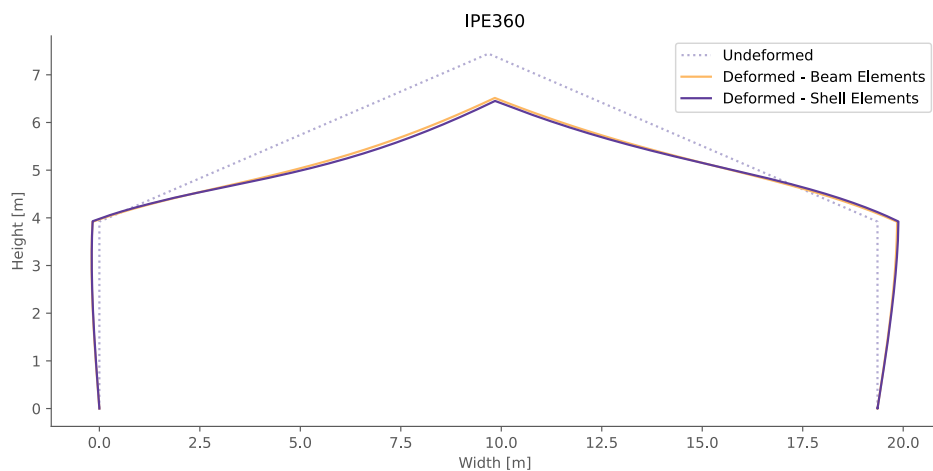


Figure 4.9: Displacement for the frame with beam-profiles IPE360 for both the two- and three dimensional model.

In addition to the deformation of the frame, the deflection along the beam was plotted for the two frames and models. The deflection of the left and right beams for the frame with beam-profiles IPE240 and IPE360 are shown in Figs. 4.10-4.13 respectively.

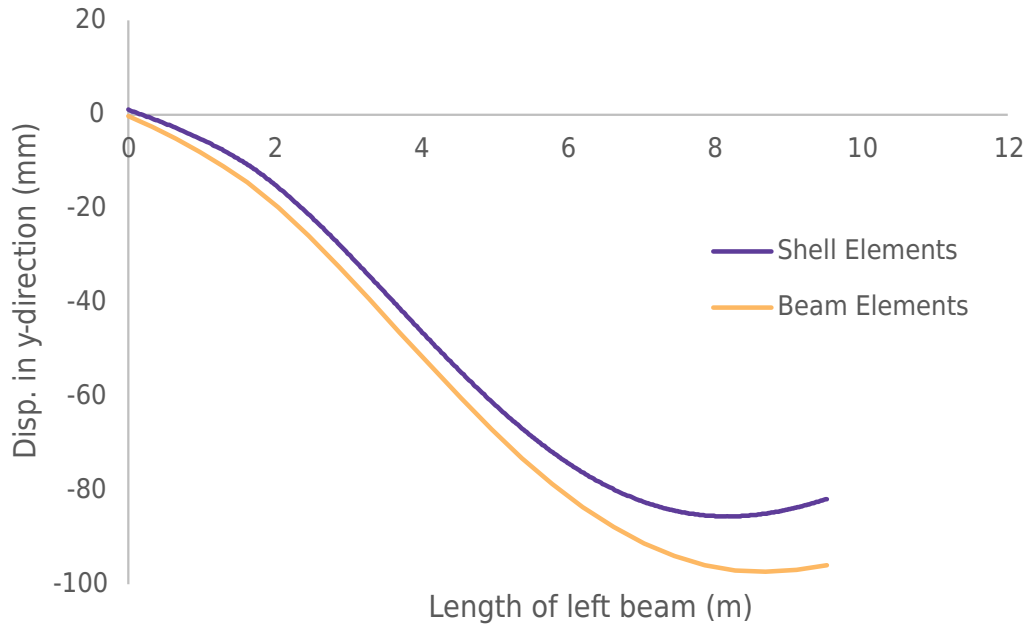


Figure 4.10: Displacement of the left beam for the frame with beam-profiles IPE240. Top of the frame is at the right. The deflection is represented by the vertical axis and the length of the beams represented by the horizontal axis.

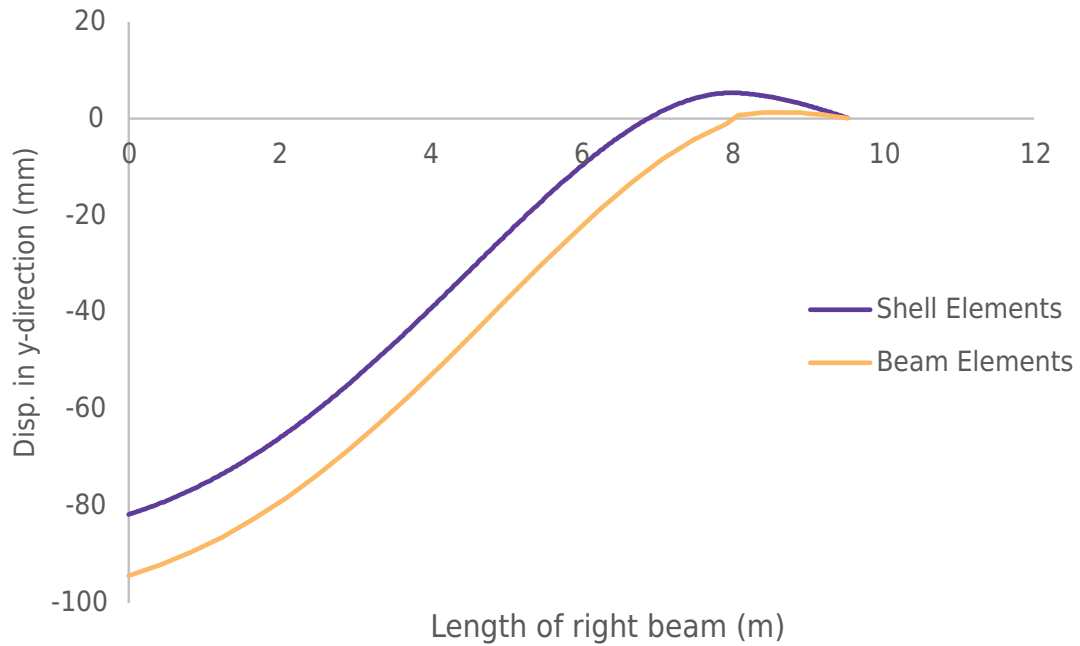


Figure 4.11: Displacement of the right beam for the frame with beam-profiles IPE240. Top of the frame is at the left. The deflection is represented by the vertical axis and the length of the beams represented by the horizontal axis.

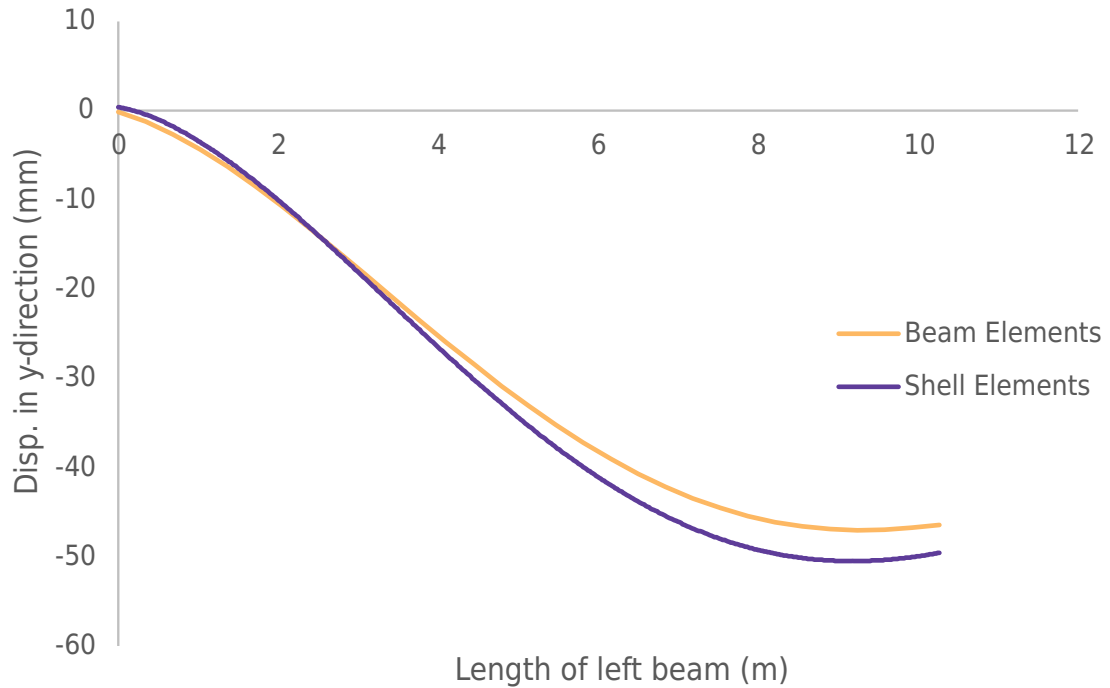


Figure 4.12: Displacement of the left beam for the frame with beam-profiles IPE360. Top of the frame is at the right. The deflection is represented by the vertical axis and the length of the beams represented by the horizontal axis.

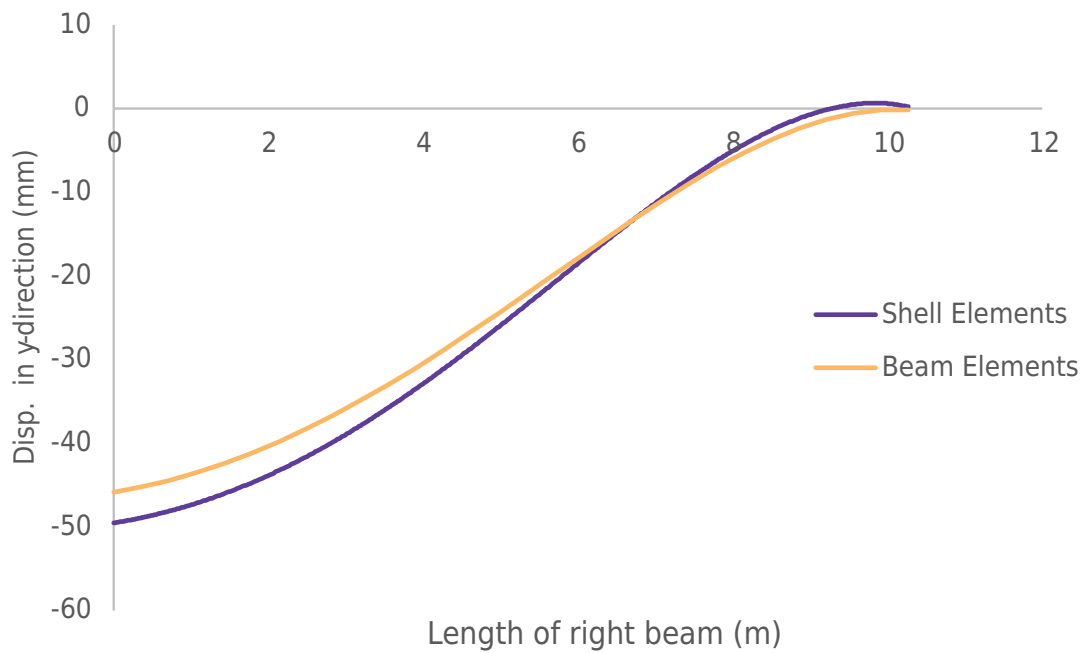


Figure 4.13: Displacement of the right beam for the frame with beam-profiles IPE360. Top of the frame is at the left. The deflection is represented by the vertical axis and the length of the beams represented by the horizontal axis.

The maximum difference in deflection for each beam and frame is presented in Table 4.3. It is observed that there is a greater difference for the frame with beam-profiles IPE240 with haunches.

Table 4.3: The difference in greatest deflection for each beam and frame.

Beam	Shell Elements [mm]	Beam Elements [mm]	Diff. [mm]	Diff. [%]
Left IPE240	-85.6	-97.4	11.8	-12.1%
Right IPE240	-81.7	-94.3	12.6	-13.3%
Left IPE360	-50.5	-47.0	-3.5	7.4%
Right IPE360	-49.6	-45.9	-3.7	8.1%

5 Critical load and utilization

A linear buckling analysis and a non-linear static analysis, with large deformations and elasto-plastic material, were performed on the three-dimensional model. This was performed to determine the critical load carrying capacity of the frames. These two critical loads will be used to compare the utilization between the two-dimensional and three-dimensional models.

5.1 Linear buckling analysis

A linear buckling analysis is performed with an eigenvalue solver to determine the critical load for the frame. The applied load is presented in section 3.2.5. The first eigenmodes for both models in the buckling analysis resulted in a failure mode that was lateral torsional buckling. The lateral torsional buckling occurred in the right beam of the frame where the lower flange displaced out of the plane. The failure modes are shown in Figs. 5.1-5.4 for the two frames.

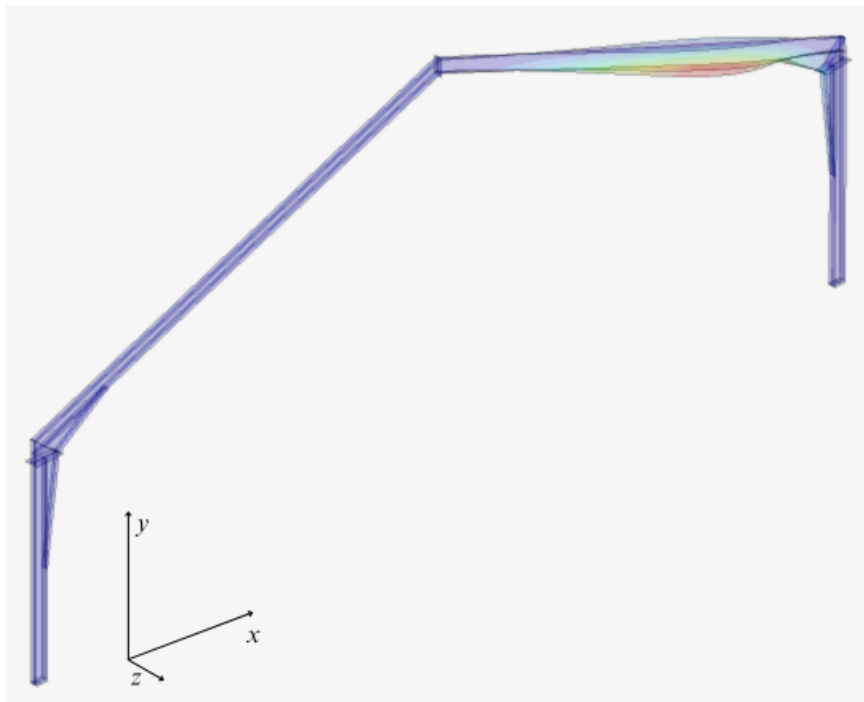


Figure 5.1: The failure mode for the lowest load for the frame with beam-profiles IPE240 with haunches. A factor has been added to enhance the lateral torsional buckling.

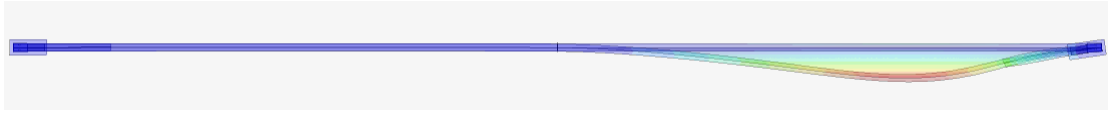


Figure 5.2: Showing the lateral torsional buckling from above for the IPE240 frame.

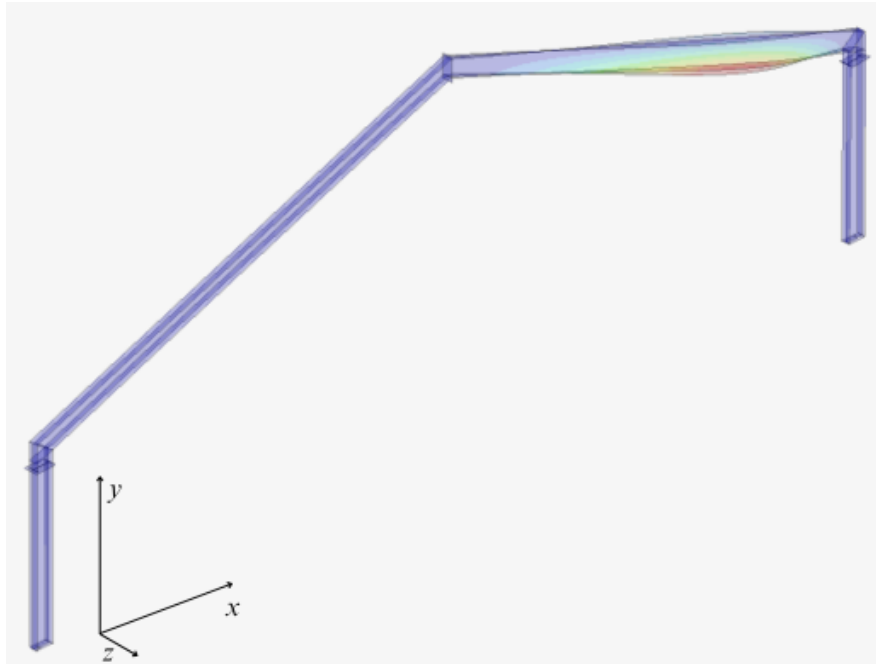


Figure 5.3: The failure mode for the lowest load for the frame with beam-profiles IPE360 without haunches. A factor has been added to enhance the lateral torsional buckling.

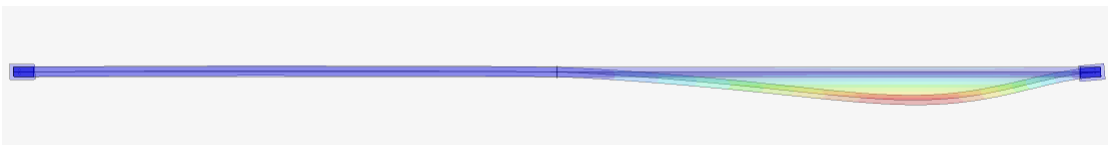


Figure 5.4: Showing the lateral torsional buckling from above for the IPE360 frame.

The critical load for this failure mode is represented by a factor of all the applied loads acting on the structure, this includes the load contributed by the structures own weight. This factor is referenced by eigenvalue or buckling load factor. For a structure with perfect geometry a value above one indicates that more load can be applied to the structure without any instability and a value below one indicates that the applied load causes instability. The utilization of the structure is calculated by dividing one by the eigenvalue. The eigenvalue for both frames is shown in table 5.1 along with the utilization in regards to stabilization.

Table 5.1: Eigenvalue and utilization.

Frame	Eigenvalue	Utilization
IPE240	1.44	69 %
IPE360	4.45	22 %

5.2 Non-linear static analysis

The non-linear analysis uses the Newton-Raphson scheme to determine the critical load for the frame. When the maximum load is reached the Newton-Raphson scheme in force control is unable to converge which is described in section 2.3.3. The Newton-Raphson scheme was unable to converge when the load as presented in Table 5.2 was applied to the frame. This critical load is presented as a critical load factor, which is a factor of the load that is applied to the frame, along with the utilization of the frame. This load factor scales the imperfection load that is applied in this analysis as well.

Table 5.2: Critical load factor and utilization for the different frames of the shell model.

Frame	Load factor	Utilization
IPE240	1.18	85 %
IPE360	2.33	43 %

The critical load factor derived from the non-linear static analysis is lower compared to the one derived from the linear buckling analysis due to plastic strains and large deformations. This comparison is illustrated in the load-displacement curves in Figs 5.5 and 5.6. The out-of-plane displacement for the lower flange was chosen due to lateral torsional buckling of the right beam being the failure mode for both frames.

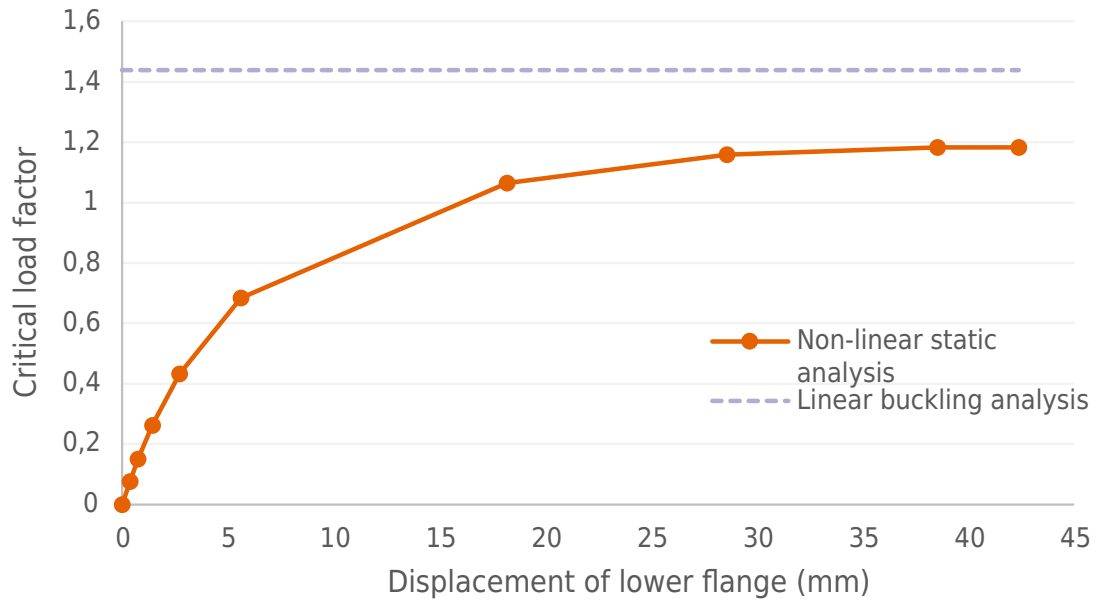


Figure 5.5: Load-displacement curve for the linear buckling and non-linear static analysis performed on the frame with beam-profiles IPE240. The critical load factor is represented by the vertical axis and the displacement of the lower flange in the middle of the right beam in the out-of-plane direction is represented by the horizontal axis.

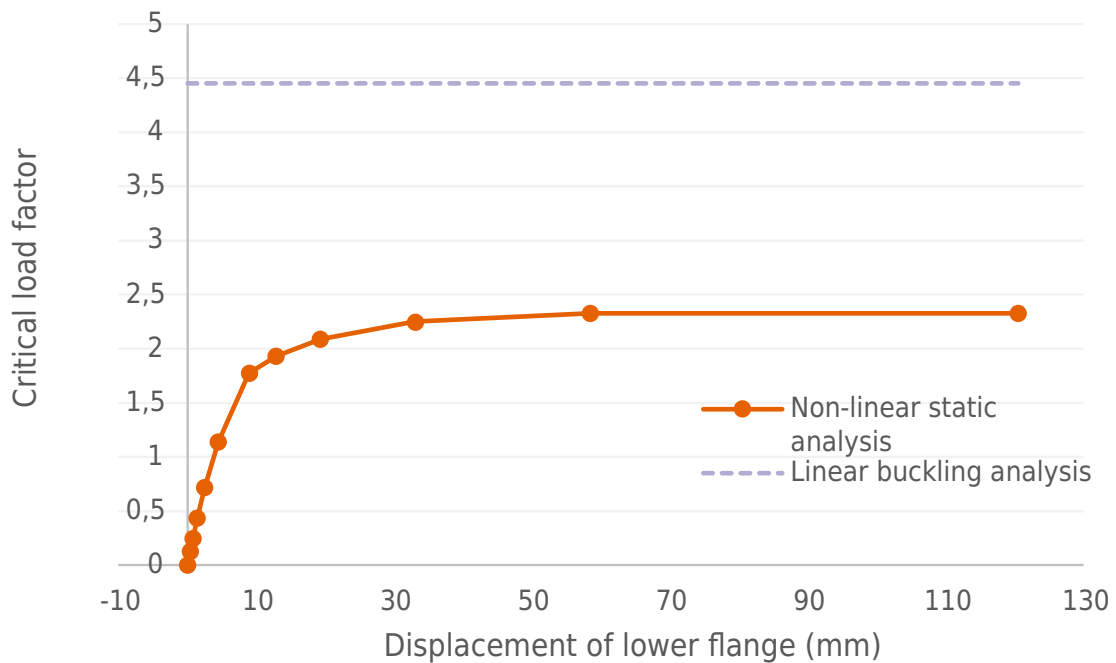


Figure 5.6: Load-displacement curve for the linear buckling and non-linear static analysis performed on the frame with beam-profiles IPE360. The critical load factor is represented by the vertical axis and the displacement of the lower flange in the middle of the right beam in the out-of-plane direction is represented by the horizontal axis.

The distribution of plastic strains in the frames occurring from the critical load is presented in Figs. 5.7 and 5.8. Local distribution of plastic strains in the corner of the frames is presented in Fig. 5.9. The frame with beam-profiles of IPE240 has no plastic strains along the whole frame except one local plastic region where the haunch connects with the beam. The frame with beam-profiles IPE360 experience more plastic strains with mainly two local plastic regions where the whole beam-profile is yielding. These local plastic regions are on the left and right side of the lateral torsional buckling of the right beam.

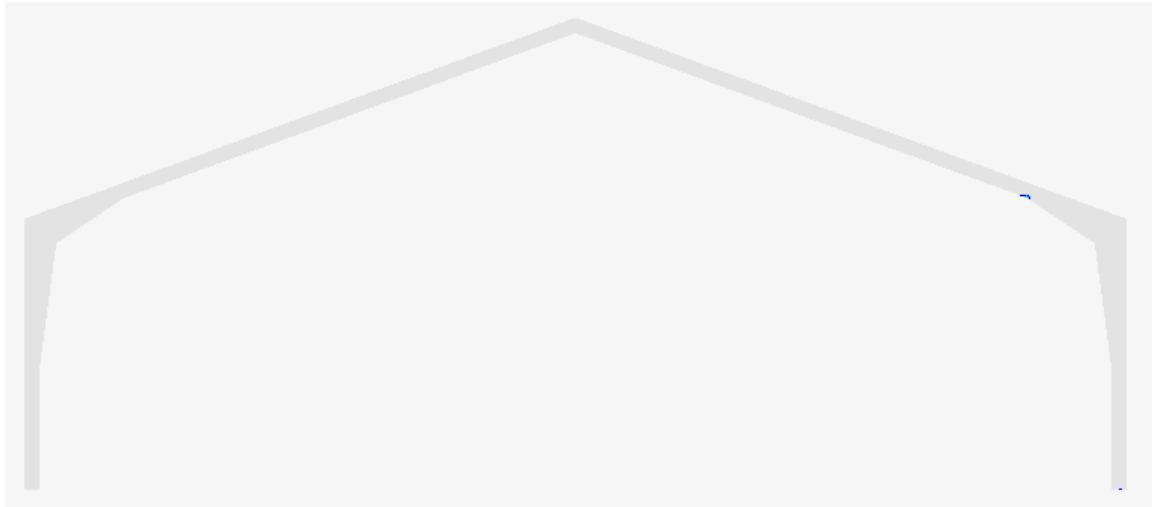


Figure 5.7: Distribution of plastic strains for the frame with beam-profiles IPE240.

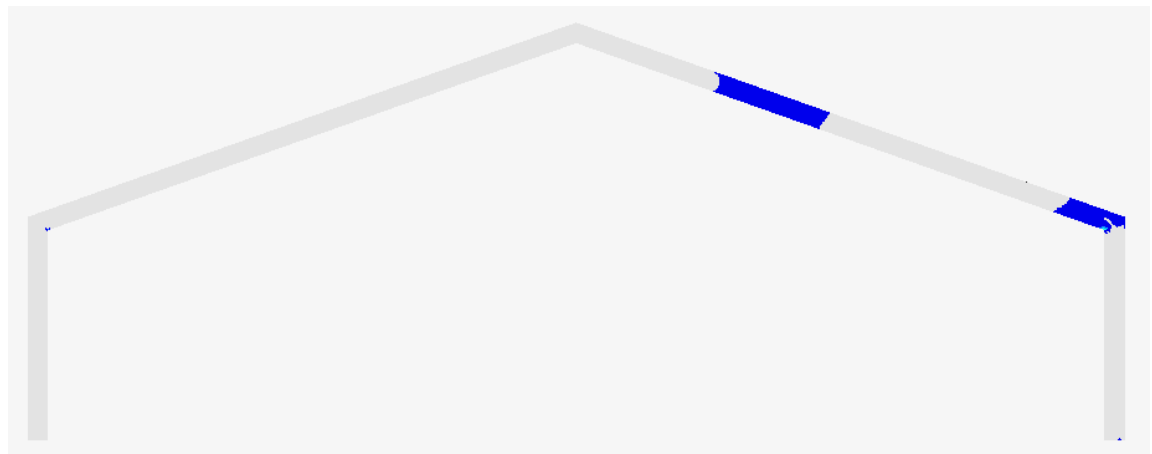


Figure 5.8: Distribution of plastic strains for the frame with beam-profiles IPE360.

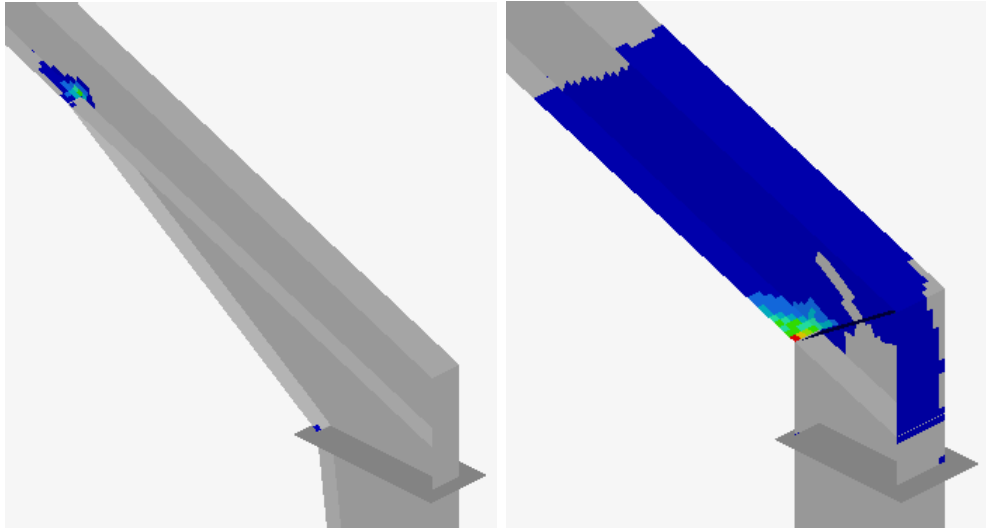


Figure 5.9: Local distribution of plastic strains in the corner of both frames. The color blue is the lowest value for plastic strains and the color red is the highest value of plastic strains.

The deformation for both frames is presented in Figs. 5.10 and 5.12 which show the lateral torsional buckling in the right beam. The deformation as seen from above is presented in Figs. 5.11 and 5.13 which shows the lateral displacement for the lower flange. The displacements are multiplied by a factor of 10 and 5 for the frames with beam-profile IPE240 and IPE360, respectively. The out-of-plane displacement of the lower flange in both frames are presented in Figs. 5.14 and 5.15 to visualize the lateral torsional buckling. The out-of-plane displacement for the lower flange is represented by the vertical axis. The length of the frame is represented by the horizontal axis.

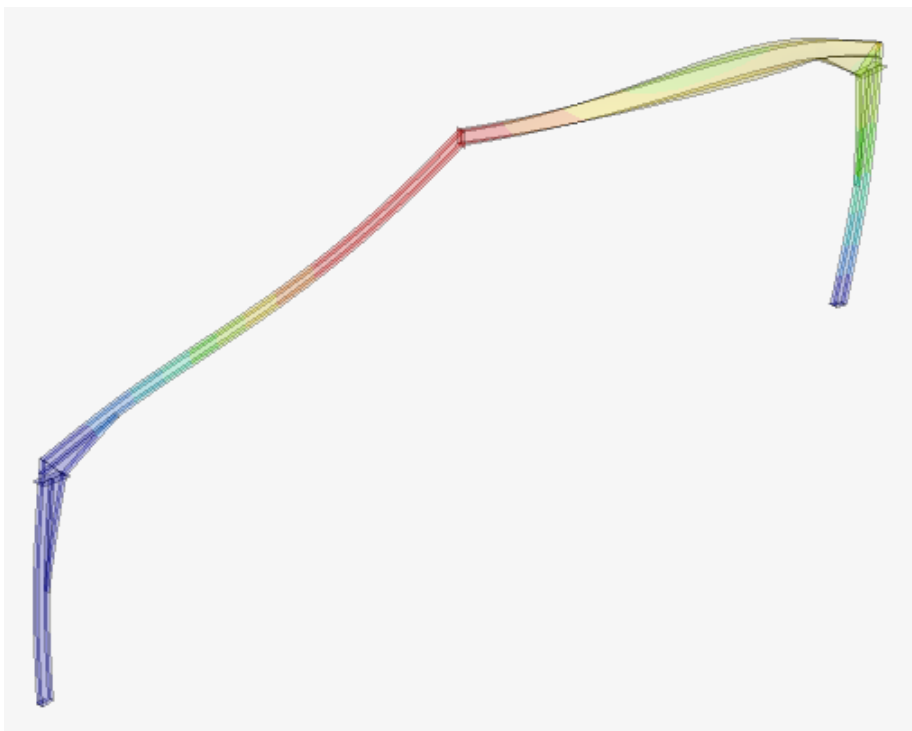


Figure 5.10: Lateral torsional buckling of frame with beam-profiles IPE240.



Figure 5.11: Lateral torsional buckling of frame with beam-profiles IPE240, seen from above.

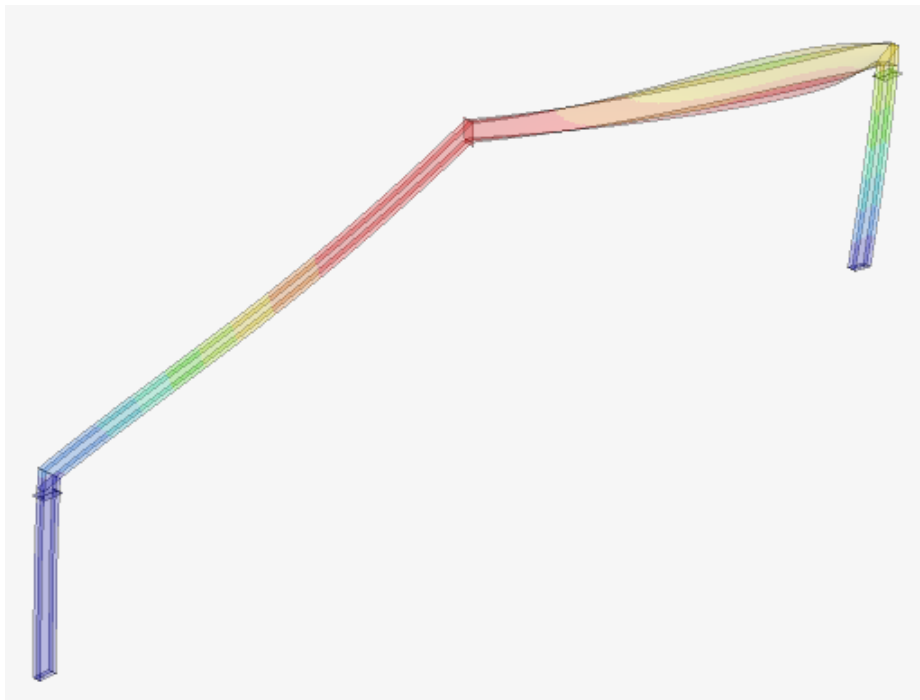


Figure 5.12: Lateral torsional buckling of frame with beam-profiles IPE360.

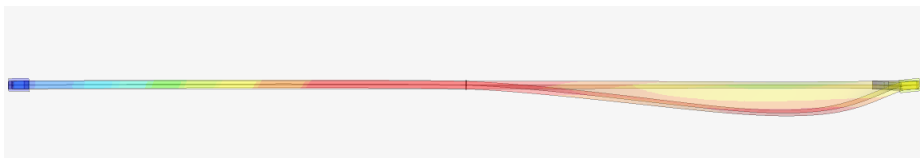


Figure 5.13: Lateral torsional buckling of frame with beam-profiles IPE360, seen from above.

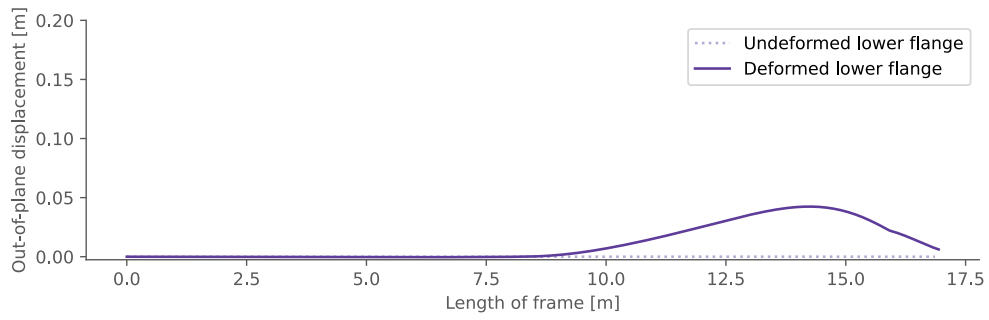


Figure 5.14: Displacement of lower flange in the beams of the frame with beam-profiles IPE240.

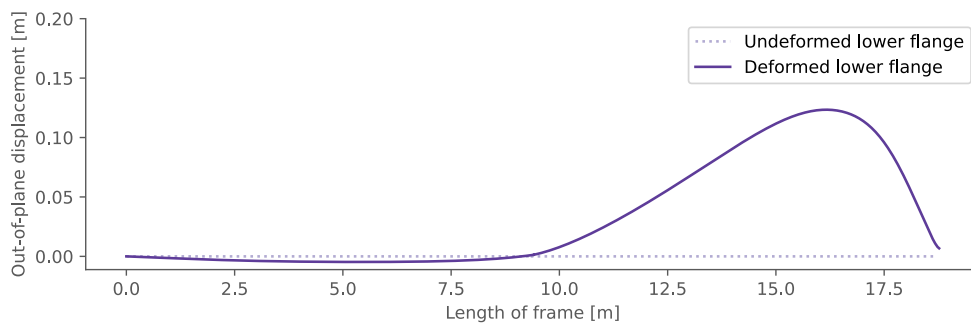


Figure 5.15: Displacement of lower flange in the beams of the frame with beam-profiles IPE360.

5.3 Comparison with the two-dimensional model

The utilization in regards to stability is calculated in the design tool according to Eqs. 2.17 and 2.18 found in section 2.2.3 using the normal forces and moments calculated from the two-dimensional model. The most utilized structural component, according to the design tool, is the right beam. This is the same structural component that is subjected to lateral torsional buckling and causes instability of the frame according to the linear buckling analysis and non-linear static analysis, performed on the three-dimensional models. The utilization for both models, including both analysis types, is presented in Table 5.3.

Table 5.3: Utilization for both models and frames.

	Beam Elements	Shell Elements Linear	Shell Elements Non-linear
IPE240	458 %	69 %	85 %
IPE360	84 %	22%	43 %

The utilization is higher for the two-dimensional model. This implies that the design tool, using this model, will suggest a larger dimension for the beam-profiles to achieve a similar utilization compared to the three-dimensional model. This is a conservative approach to stabilizing the frame and will put a higher demand on the use of material.

6 Improvements to existing model

The design tool, using the two-dimensional model, was established to be conservative. In the following chapter the results from two suggested improvements are presented along with the methods to implement these improvements. The first improvement is in regards to applying the Eurocode. The second improvement is in regards to improving the stability for the frames and how this is modelled.

6.1 Considering moment distribution in stability analysis

The equation for calculating stability utilization according to Eurocode was performed for the beam model as described in section 2.2.3 and Eqs. (2.17) and (2.18). In both these equations the critical elastic lateral torsional buckling moment, M_{cr} , must be calculated. This equation is taken from a national appendix [17] and is presented in Eq. (6.1)

$$M_{cr} = C_1 \frac{\pi^2 EI_z}{L^2} \sqrt{\frac{I_w}{I_z} + \frac{L^2 GI_t}{\pi^2 EI_z}} \quad (6.1)$$

where Young's modulus is denoted E and the moment of inertia around the weak is denoted I_z , according to Fig. 6.1. The beam length between points, which have lateral restraints, is denoted L and is the length of the right beam for this case see Fig 6.2. The torsion constant is denoted I_t and the warping constant is denoted I_w . The coefficient C_1 depends on the section properties, support conditions and the moment diagram. In the design tool the members of the structure are seen as only having end moments, illustrated in Fig. 6.1, and the parameter, C_1 has been set to be equal to one implying that the ratio of the end moments, ψ are equal to one [17]. In Figs. 4.6 and 4.7 the moment distributions for the right beams, where lateral torsional buckling occur, is presented with moment diagrams and shows that the ratio between the end moments are not equal to one. This is illustrated in Fig. 6.2 and the ratio can be calculated according to Eq. (6.2) and the results are presented in Table. 6.1 for both frames and models.

$$\psi = \frac{M_{left}}{M_{right}} \quad (6.2)$$

Because the end moment ratio, ψ is not equal to one a higher value for the parameter, C_1 should be chosen to be more accurate. If the value of C_1 would increase the value of M_{cr} will also increase at the same rate, which is used to calculate the slenderness index, $\bar{\lambda}_{LT}$ according to Eq. (6.3).

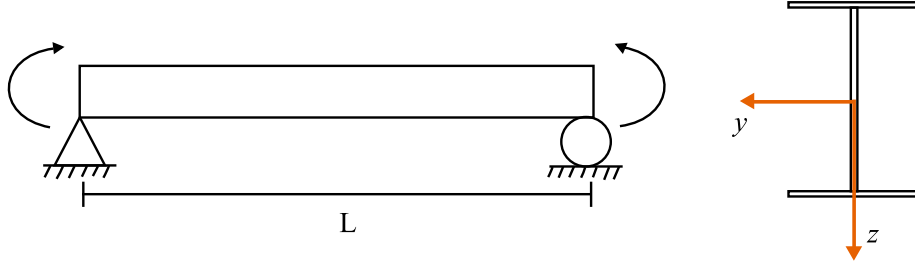


Figure 6.1: End moment acting on the structural component and the cross-section where y -axis and z -axis are displayed.

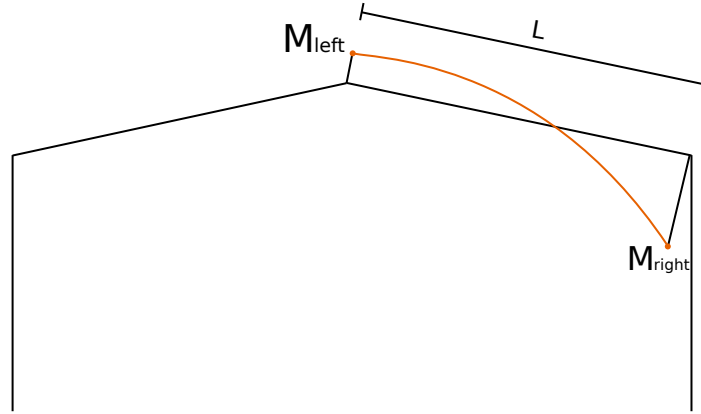


Figure 6.2: Moment distribution of the right beam and defined end moments.

Table 6.1: Result of the calculation of the end moment ratio in the different frames

Frame	Moment Ratio ψ beam model	Moment Ratio ψ shell model
IPE240	-0.21	-0.16
IPE360	-0.33	-0.29

$$\bar{\lambda}_{LT} = \sqrt{\frac{W_y f_y}{M_{cr}}} \quad (6.3)$$

The slenderness index is then used in Eq. (6.4) and then Eq. (6.5)

$$\Phi_{LT} = 0.5 [1 + \alpha_{LT}(\bar{\lambda}_{LT} - 0.2) + \bar{\lambda}_{LT}^2] \quad (6.4)$$

$$\chi_{LT} = \frac{1}{\Phi_{LT} + \sqrt{\Phi_{LT}^2 - \bar{\lambda}_{LT}^2}} \quad (6.5)$$

where α_{LT} is an imperfection factor. Lastly, the result from Eq. (6.5) is used in Eqs. (2.17) and (2.18) found in section 2.2.3. From these equations it can be proven that an increasing value of C_1 will lead to a decreasing value of the utilization regarding stability. Thus making the choice of setting C_1 equal to one very conservative.

Other parameters that will have an impact on the stability utilization, calculated according to Eurocode, are the interaction factors k_{yy} and k_{zz} [10]. A lower value for

the interaction factors will lead to a lower utilization in regards to stability. These are both calculated with the Eq. (6.6)

$$k_{ii} = C_{mi} \left(1 + 0.6\bar{\lambda}_i \frac{N_{Ed}}{\chi_i N_{Rk} / \gamma_{M1}} \right) \quad (6.6)$$

where C_{mi} is calculated according to Eq. (6.7)

$$C_{mi} = 0.79 + 0.21\psi_i + 0.36(\psi_i - 0.33) \frac{N_{Ed}}{N_{cr,i}} \quad (6.7)$$

where the end moment ratio is denoted ψ_i , which is calculated in Eq. (6.2). The design normal force is denoted N_{ed} and the elastic critical load is denoted $N_{cr,i}$. From Eqs. (6.6) and (6.7) it is shown that the interaction factors will decrease in value if the value for end moment ratio decreases.

Thus the two main factors that will have an impact on the utilization in regards to stability for the frames will be the parameter C_1 and the end moment ratio ψ . The impact a higher value for the parameter C_1 and a correct lower value for the end moment ratio ψ had on the utilization for the frame was investigated. The utilization was calculated with the design tool, using the two-dimensional model using beam elements, varying the parameter C_1 . This was performed two times, one with the end moment ratio set to be equal to one and one where the end moment ratio was set to the actual value. How the utilization in regards to stability for both frames is dependent on these two values are shown in Figs. 6.3 and 6.4. The utilization is represented by the vertical axis and the parameter C_1 is represented by the horizontal axis. The purple line is using the end moment ratio ψ that is equal to one and the light purple line a value that is equal the actual value derived from the two-dimensional model. The yellow dotted line shows the utilization derived from the non-linear analysis using the three-dimensional model using shell elements.

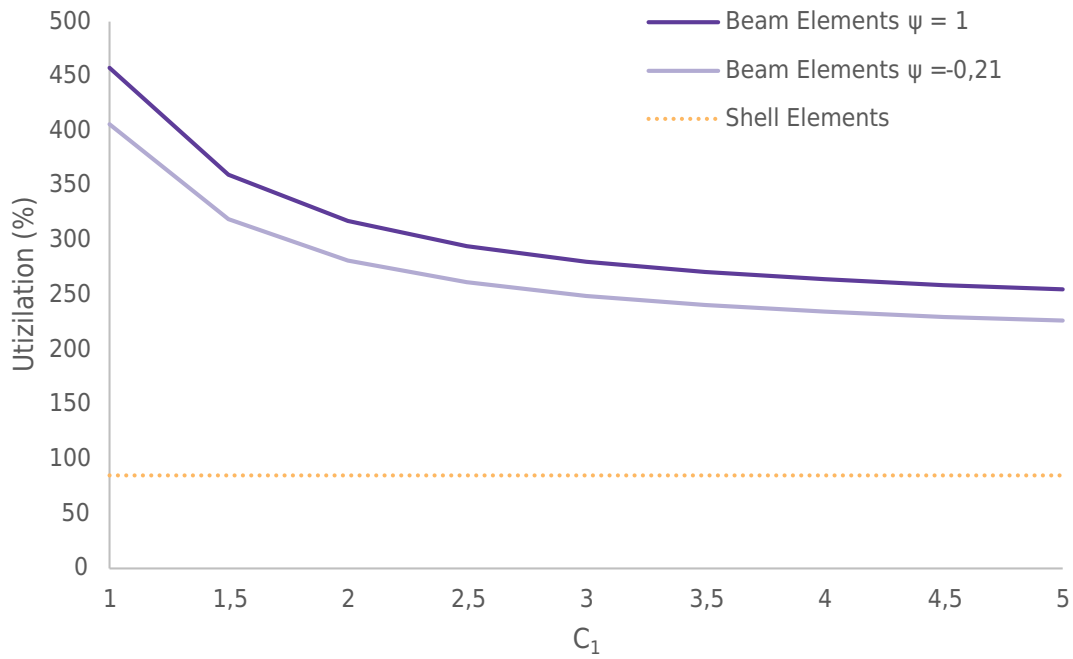


Figure 6.3: The effects on utilization for the frame with beam-profiles of IPE240 when choosing different values for C_1 and ψ .

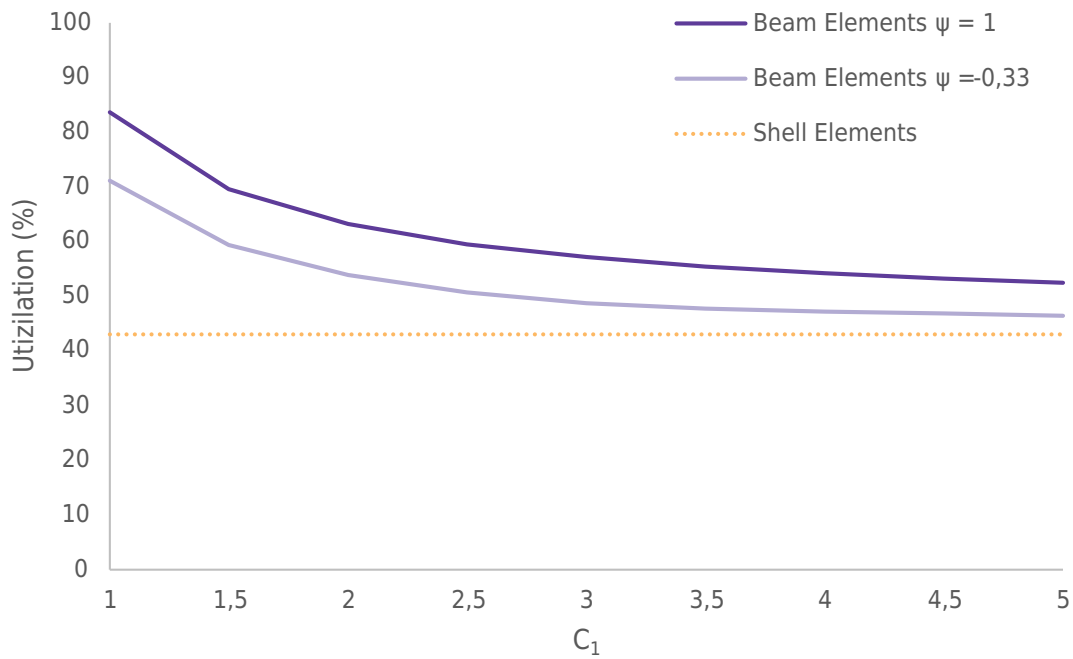


Figure 6.4: The effects on utilization for the frame with beam-profiles of IPE360 when choosing different values for C_1 and ψ .

6.2 Rigid connections between beam and purlins

It was investigated how the connection between beams and purlins contributes to the stability of the frame. According to how the frames are built on-site, the beam and purlin connections at the top and at the corner are connected with two bolts instead of one, as it is for the other beam and purlin connections. The location is shown in Fig. 6.5. The double bolted connection is shown in Fig. 6.6 and is considered a rigid connection. When the load from wind and snow give rise to torsion of the beam, the purlins resist this motion due to the bending stiffness of the purlins. These connections are not taken into consideration in the two-dimensional design tool using beam elements.

To imitate this resistance caused by the bending stiffness of the purlins the connection between the purlins and frame were modelled as rotation springs which is shown in Fig. 6.6. This was performed to achieve additional rotational stiffness at the points where this connection is used. The spring stiffness is derived from Eq. (6.8)

$$M = k \cdot \theta \quad (6.8)$$

where the rotational stiffness is denoted k , the moment denoted M and the rotational angle is denoted θ . With elementary case according to Fig. 6.7 where moment is set for a rotation that is equal to one the rotational stiffness can be calculated using Eq. (6.9)

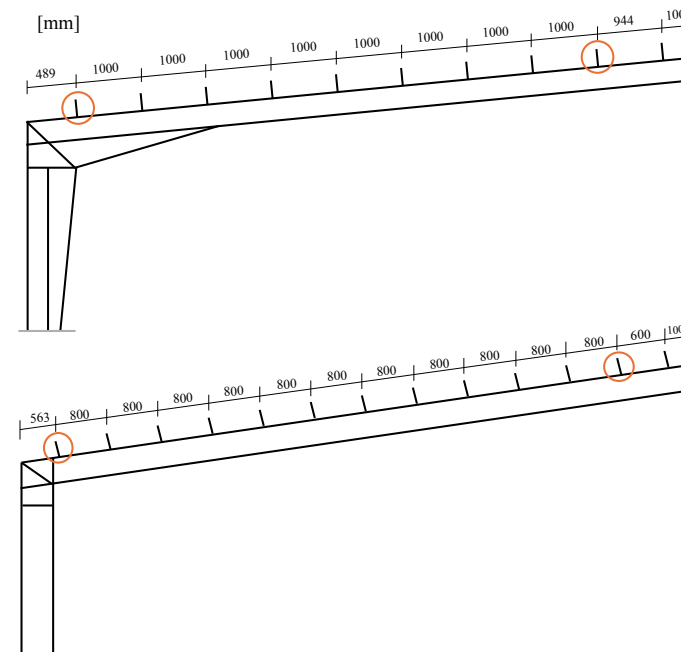


Figure 6.5: Placement of purlins on top of the beam. The two marked connections are double bolted. Recreated from blueprints.

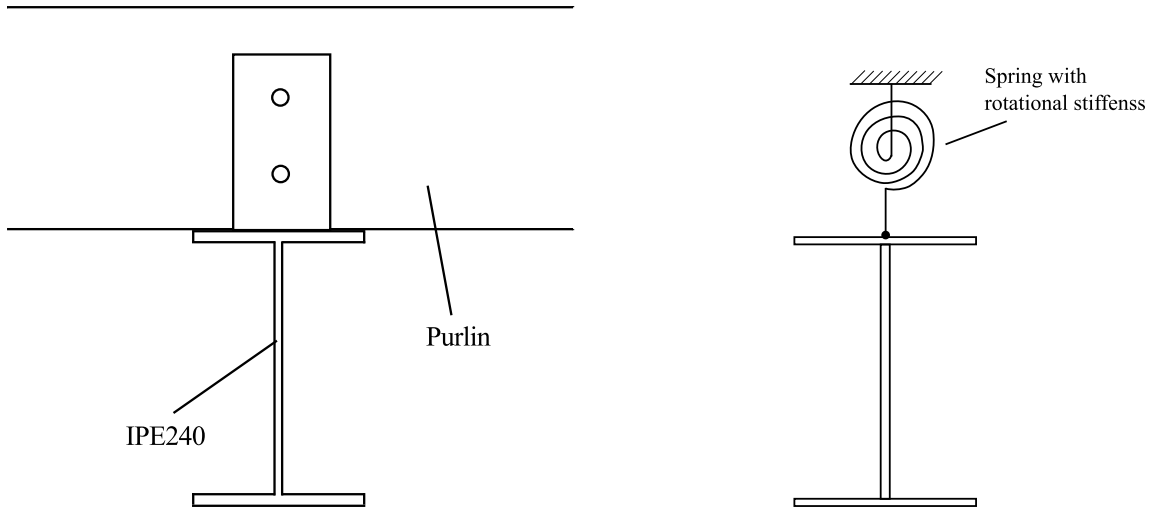


Figure 6.6: Connection between beam and purlin for a beam-profile IPE240 and how they are modelled with springs.



Figure 6.7: The elementary case that was used for calculating the spring stiffness in the modeled purlins.

$$k = 2 \cdot \left(\frac{3 \cdot EI}{L} \right) \quad (6.9)$$

where the modulus of elasticity for the material used for the purlins is denoted E . The moment of inertia is denoted I and the length of the purlin is denoted L . The material used for the purlins are timber of the type C24 thus the elasticity modulus is set to 7400 MPa [18]. The rotational stiffness is multiplied by a factor of 2 as there are two purlins at each side of the beam that will add to the rotational stiffness. The moment of inertia, I , is calculated according to Eq. (6.10)

$$I = \frac{b \cdot h^3}{12} \quad (6.10)$$

where the width of the cross-section for the purlin is denoted b and the height of the cross-section is denoted h . For both frames, purlins with a rectangular cross-section were used. For the frame with beam-profiles of IPE240, purlins of the dimension 45×195 mm were used and for the frame with beam-profiles IPE360, purlins of the size 45×220 mm were used.

The effect modelling this rigid connection had on stability and also the utilization was studied by performing a linear buckling analysis on the three-dimensional model. The linear buckling analysis was performed when the connections, as the connections are today, were modelled as rigid but also the effect when more connections could be seen as rigid. This implies a change of single bolted to double bolted connection

between purlin and beam. The placements of these rigid connections and how they are distributed along the beams of the frame are seen in Fig. 6.8.

The added rotational stiffness provided by the purlins connection to the beam is not around the global x -axis as the beam is at an angle. Two local coordinate systems, one for each beam, were introduced where the y -axis was normal to the outer flanges and the x -axis along the length of the beam. The rotational stiffness was applied around this local x -axis. The result from the linear buckling analysis with the rotational springs implemented is presented in Tables 6.2 and 6.3 showing the eigenvalues and failure modes and in Figs. 6.9 and 6.10 showing the effect on utilization.

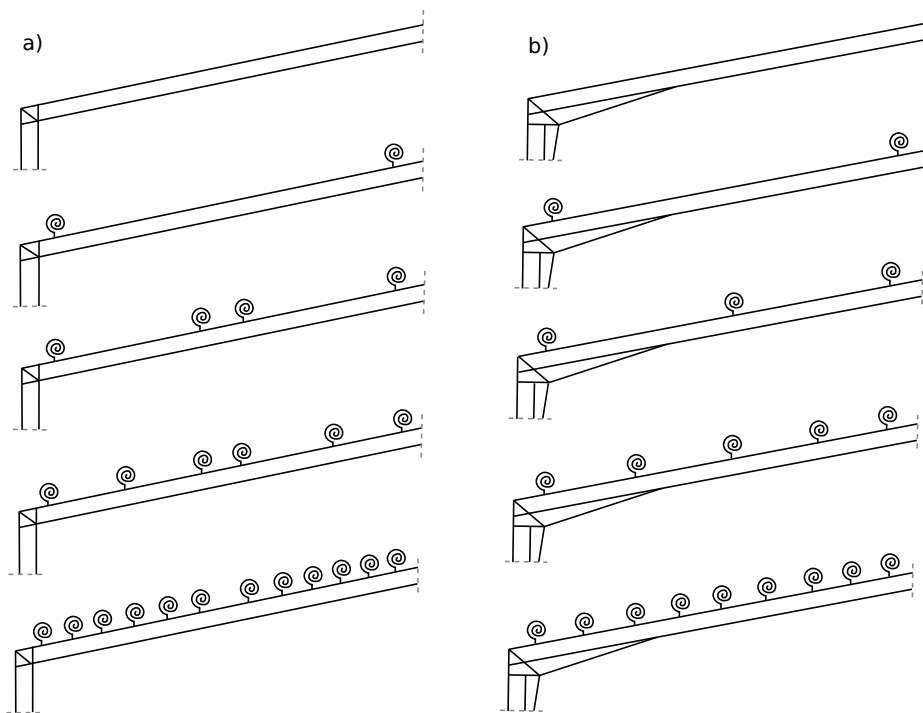


Figure 6.8: Analysis performed with various positions of springs added in the shell model a) for the IPE360 frame and b) IPE240.

Table 6.2: The result of a linear buckling analysis for different number of springs along the left and right beam in the frame with beam-profiles of IPE240. LTB stands for later torsional buckling.

Number of Springs	Eigenvalue	Failure mode
0	1.44	LTB in beam
2	1.49	LTB in beam
3	1.90	LTB in beam
5	2.72	LTB in columnn
9	2.72	LTB in columnn

Table 6.3: The result of a linear buckling analysis for different number of springs along the left and right beam in the frame with beam-profiles of IPE360. LTB stands for later torsional buckling.

Number of Springs	Eigenvalue	Failure mode
0	4.45	LTB in beam
2	4.65	LTB in beam
4	6.46	LTB in beam
6	7.95	LTB in beam
12	8.96	LTB in columnn

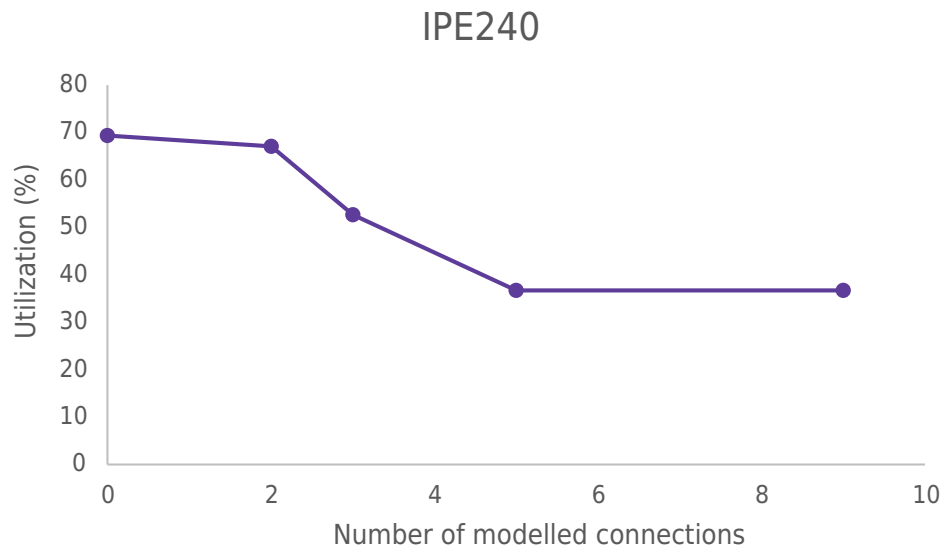


Figure 6.9: The effect modelling rigid connections as rotational springs has on the utilization of the frame in regards to stability. Frame with beam-profiles IPE240.

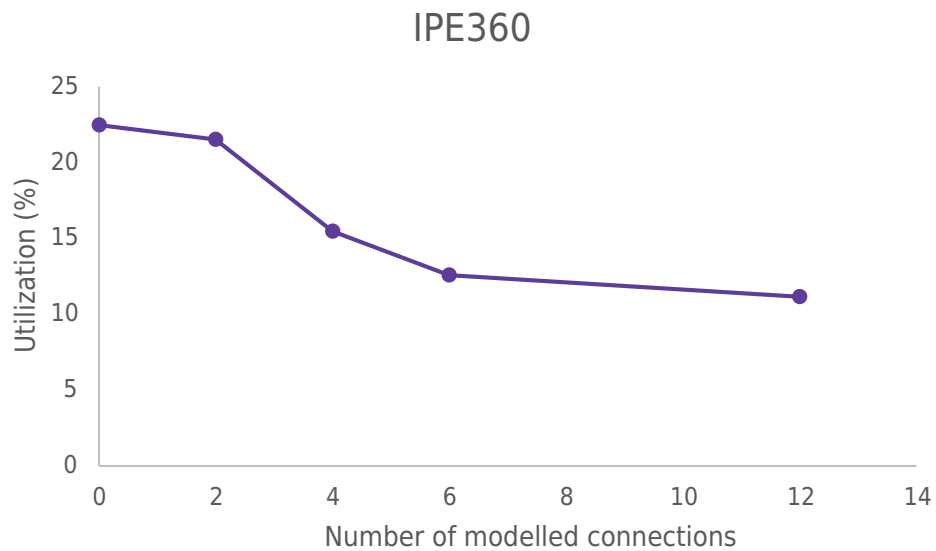


Figure 6.10: The effect modelling rigid connections as rotational springs has on the utilization of the frame in regards to stability. Frame with beam-profiles IPE360.

7 Discussion

7.1 Comparison between the two models

When comparing the two models, one using beam elements and the other using shell elements, there are small differences in reaction forces, normal force distributions and displacements. The reaction forces differ less in the y -direction than in the x -direction. Difference in reaction forces indicates that the applied forces in the two models are not entirely equal. This is believed to be caused by an error when translating the geometries of the different models. Although, the root of the issue is however not found despite troubleshooting. The same parameters were used when calculating the snow load and wind load according to Eqs. (3.7) and (3.2) found in section 3.2.5. The width and height for the model using shell elements were believed to be implemented correctly in the design tool and the troubleshooting stopped here. For further investigation the calculations of snow and wind load in the design tool needs to be reviewed. As the difference is at its highest at 9,2 percent and lowest at 1.7 percent, whereas the result from stability utilization differs substantially more, it can be accepted.

The final boundary condition that was chosen to represent a pinned column-to-ground connection was to restrict only the holes for bolts in translation in all directions. It was observed that when the flanges were restricted in the vertical direction it became increasingly more similar to a fixed column-to-ground connection, compared to a fixed boundary condition applied in the design tool. The last examined boundary condition being very similar. This boundary condition was not expected to behave like a pinned column-to-ground connection, but to visualise the different options for restrictions for the ground plate.

When comparing the deflection between the two models, two different behaviours was observed from the two different frames. The deflection for the two-dimensional model was higher than the three-dimensional model for frame with beam-profiles of IPE240. The deflection for the two-dimensional model was lower than the three-dimensional model with beam-profiles of IPE360. Because the normal forces are greater in the three-dimensional model, the deflection was expected to be slightly higher. This behaviour is seen for the second frame with no haunches but the opposite for the first frame with haunches. This is believed to be caused by the modelling differences of the corners. The stiffness, which is influenced by the haunches, are believed to be higher for the three-dimensional model using shell elements. In the design tool the method for considering the implementation of haunches is to elongate the web of the IPE-profile. In the more detailed three-dimensional model the implementation of haunches is considered more realistically where a haunch is added to the IPE-beam. Using shell elements instead of beam elements allows for this modelling. Respective details can be seen in Figs. 3.2 and 3.3 found in sections 3.1.1 and 3.2.2. The added stiffness from a flange is therefore disregarded in the two-dimensional model using beam elements.

7.2 Critical load

The critical load for the frame with beam-profile IPE240 derived from the linear buckling analysis is higher than the one derived from the non-linear static analysis. There is a greater difference when the two analysis are performed for the frame with beam-profiles IPE360. The critical load derived from the linear buckling analysis for that frame is about double the critical load from the non-linear static analysis. The linear buckling analysis does not consider the plasticity of the material as the behaviour of the material in this analysis was elastic. In the non-linear static analysis the material of the frame has plastic behaviour above the yielding limit. When the material yields at local places of the frame, the frame becomes less stiff and the load path changes. This behaviour happens gradually in the non-linear static analysis whereas for the linear buckling analysis this behaviour happens abruptly, due to the eigenvalue method.

The difference between the two analyses in regards to critical load is greater for the frame with beam-profiles of IPE360 than beam-profiles of IPE240. The first mention frame has more plastic strains when the critical load is applied. This phenomenon is disregarded in the linear buckling analysis which causes the difference between the two frames. This suggest that the frame with the beam-profiles IPE240 is slender and the frame with the beam-profiles IPE360 is less slender.

The failure mode associated with the critical load is lateral torsional buckling for both frames using both analysis types. The failure mode is reached sooner for the non-linear static analysis as the stiffness of the right beam decreases with the plastic strains.

7.3 Utilization in stability analyses

The design tool calculates the utilization regarding stability conservatively, with a factor between approximately 2 and 6,5 depending on the frame and analysis type. This is believed to be caused by the neglecting the moment variation along the frame. For this load case it is especially the moment variation in the right beam. The suggested improvement is to choose a higher value than one for the parameter C_1 , which takes moment distribution into consideration. The consequences of setting C_1 equal to one is assuming that the moment distribution is uniform. This means that the maximum moment will be applied uniformly along the beam when calculating the utilization in regards to stability. From both models it is observed that the moment will differ along the beam for both frames. Thus making the choice of setting C_1 equal to one incorrect. As mentioned before the design tool uses the national appendix to determine this parameter which is used to determine the critical elastic lateral torsional buckling moment, M_{cr} . This value should be carefully chosen to avoid a value too low that is more conservative than it needs to be. As lateral torsional buckling is the failure mode, the term in the stability utilization calculation, which takes lateral torsional buckling into consideration, is dominant. This implies that a change of a this coefficient is significant for the final result. For both frames the utilization decreased with higher values for parameter C_1 and even more with a correct value for the end

moment ratio ψ . For the frame with beam-profiles IPE360 the utilization, derived from the two-dimensional model, approached the utilization, derived from the three-dimensional model. For frame with beam-profiles IPE240 the utilization never reached a similar value for higher values of C_1 . This is believed to be caused by the design tool not considering the contribution from haunches to the stability of the frame.

Alternatively, to determine the utilization regarding stability of the frame with higher accuracy another method or model could be used. The method could be by using an eigenvalue problem performed in the same manner as described in section 2.3.5. Another model could be the one created using shell elements. Performing a non-linear static analysis on this model gives the most accurate result for utilization regarding stability, according to this study.

7.4 Modelling of rigid connections between beam and purlins

By modelling the connection between beams and purlins at two places per beam, the increase of buckling load is not as noticeable as when modelling three or more connections. The increased rotational stiffness at the end of the beams does not prevent the lateral torsion buckling happening near the middle of the beam. When the rotational stiffness increases in the middle of the beam the prevention against lateral torsion buckling is higher which is seen by the change of buckling load for the frames. When every other, and every connection between beam and purlins for frames with dimension IPE240 and IPE360 respectively is modelled as a rigid connection the failure mode is lateral torsion buckling in the column.

The connections are only double bolted at the ends of the beams which allows for a rigid connection to be modelled. There is a possibility to use double bolted connections for all beam-to-purlin connections. The linear buckling analysis with more rigid connections was done to examine the effect more double bolted connections would have on the stability. With enough rigid connections the failure regarding stability is not due to lateral torsion in the beam but rather in the column. Implementing this method has the possibility to decrease the need for material as a smaller dimensions might be sufficient for stability requirements and the need for lateral braces.

8 Conclusions

The conclusions of this master's thesis is presented in bullet form below.

- Modelling the frame with beam elements is sufficient to calculate the cross-section forces for frames with and without haunches and displacements for frames without haunches.
- Haunches could be implemented using a more accurate method in order to calculate the displacements more exactly.
- The design tool is conservative with a factor of 2 to 6.5 compared to the three-dimensional model depending on the frame analysis type when calculating the utilization of the frame regarding stability.
- When moment distribution is considered when using Eurocode to calculate the utilization in regarding stability, the designing is not as conservative.
- The design tool needs to consider the haunches' contributions to the stability of the frame to be more accurate when calculating the utilization.
- Incorporating rigid connections between beams and purlins, as the examined frames are constructed with rigid connections at only two positions per beam, would have a low effect on the stability.
- Creating rigid connections between beams and purlins, using two bolts instead of one, for more than two connections per beam would increase the stabilization of the frame.

9 Further studies

In order to be more sure regarding the findings of this study it would be preferable to compare with more frames, thus making a parameter study. With modelling of more frames a correlation might be found. This would be done by changing one parameter at the time and run the same analysis that has been done during this study. The parameters could be span width, size of haunches or dimensions of cross-sections. From these results, perhaps a general statement could be made regarding frames that are slender, have haunches or have a large spans if the result achieved from this study was found for several frames.

A similar study could be made including all load cases to investigate if the two-dimensional model is sufficient for all load cases. The same argument could be made for both boundary conditions. The same study could be made using fixed boundary conditions as this can be chosen in the design tool. This would increase the verification of the three-dimensional model.

One of the findings in this study was that the modelling of stiffness of the haunches lacks accuracy resulting in a larger deflection compared to the three-dimensional model. It was also mentioned that the contribution to stability from the haunches is disregarded in the design tool, using the two-dimensional model. This resulted in a larger difference between the improved utility and the original utility compared to the frame with no haunches. No further improvements on how to model the stiffness more accurately or how to consider the haunches contribution to stability were suggested. This requires a new study to suggest these kinds of improvements.

In this study it was implied that the use of material could be reduced if suggested improvements were implemented. However, a precise value of the amount of material was not given. A calculation of how much material the new improved model would save was not conducted and is up to further studies to discover.

Bibliography

- [1] Kim J. Sovacool B. K. Bazilian M. Griffiths S. Lee J. Yang M. I& Lee J. *Decarbonizing the iron and steel industry: A systematic review of sociotechnical systems, technological innovations, and policy options*. Energy research I& Social Science. Volume 89, 2022.
- [2] Holappa L. ‘A General Vision for Reduction of Energy Consumption and CO2 Emissions from the Steel Industry’. In: *Metals* (2020), p. 21.
- [3] Boverket. *Erfarenheter från takras i Sverige vintrarna 2009/10 och 2010/11*. M2010/2276/H. Karlskrona, 2011.
- [4] Johansson C.J. Lidgren C. Nilsson C. Crocetti R. *Takras vintrarna 2009/2010 och 2010/2011 - Orsaker och förslag till åtgärde*. SP Technical Research Institute of Sweden, Borås, 2011.
- [5] Hansen K. *Basic Steel Construction*. De Gruyter Berlin, 2017.
- [6] Åsted B. ‘Stålets Egenskaper’. In: *stålbyggnadsinstitutet* (2009), p. 5.
- [7] Burström P.G. *Byggnadsmaterial - Uppbyggnad, tillverkning och egenskaper*. Studentlitteratur AB, 2007.
- [8] Ioannis V. Ermopoulos J. Ioannidis G. *Design of Steel Structures to Eurocodes*. Springer International Publishing, 2019.
- [9] Runesson K. Samuelsson A. Wiberg N. E. *Byggnadsmekanik Knäckning*. Studentlitteratur Lund, 1992.
- [10] SS-EN-1993-1-1:2005. *Eurocode 3: Design of steel structures – Part 1-1: General rules and rules for buildings*. Stockholm: SIS, Swedish Standards Institute, 2008.
- [11] Saabye Ottosen N. Petersson H. *Introduction to the finite element method*. Prentice Hall, 1992.
- [12] Krenk S. *Non-linear modeling and analysis of solids and structures*. Cambridge University Press, 2009.
- [13] Saabye Ottosen N. Ristinmaa M. *The Mechanics of Constitutive Modelling*. Elsevier Ltd, 2005.
- [14] Månsson J. Nordbeck P. *Linjär algebra*. Studentlitteratur AB, 2019.
- [15] SS-EN-1991-1-4:2005. *Eurocode 1: Actions on structures – Part 1-4: General actions - Wind actions*. Stockholm: SIS, Swedish Standards Institute, 2008.
- [16] SS-EN-1991-1-3. *Eurocode 1: Actions on structures – Part 1-3: General actions - Snow loads*. Stockholm: SIS, Swedish Standards Institute, 2005.
- [17] Bureau A. *NCCI: Elastic critical moment for lateral torsional buckling, SN003a-EN-EU*. <https://dan.ct.upt.ro/fire/files/NCCI-SN003a-EN-EU.pdf>, 2008.
- [18] Svenskt Trä. *TräGuiden*. <https://www.traguiden.se/konstruktion/dimensionering/hallfasthet-och-barformaga/karakteristisk-hallfasthet/konstruktionsvirke2/>, 2019.

Appendix A

A.1 Effects of different boundary conditions

When modelling a three-dimensional model the boundary conditions are of great importance. This is why two additional boundary conditions were applied to investigate the difference in reaction forces. As mentioned before, the first way to model the connection between the ground and column was to only restrain the holes in all displacement directions. The second chosen boundary condition was to restrain all translation around the holes and translation in y -direction for the outer flange of the column. The boundaries are visualized in Fig. A.1. With this boundary condition the result of the reaction forces are presented in table A.1 and table A.2 for the two different frames.

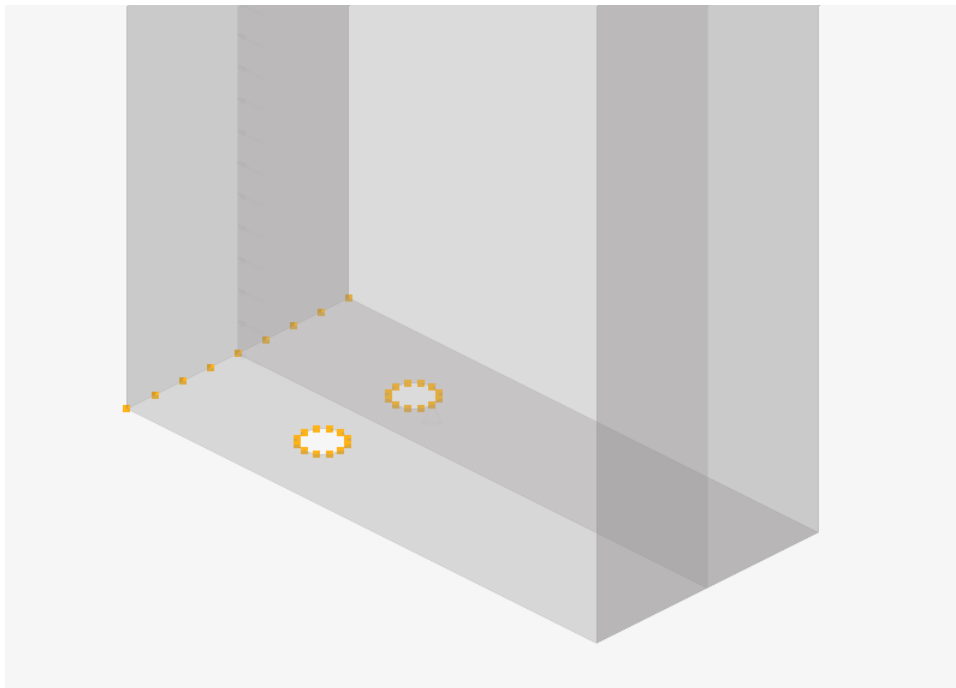


Figure A.1: Clarification of the second boundary condition. Translation in all directions are constrained around the holes and translation in y -direction is constrained for the outer flange.

Table A.1: Reaction forces for models using shell and beam elements for a frame with beam-profiles IPE240 with haunches, both holes and outer flange restricted in translation.

Left support	Shell Elements [kN]	Beam Elements [kN]	Diff. [kN]	Diff. [%]
x - direction	32.9	26.5	6.4	24.2%
y - direction	66.7	64.2	2.5	3.9%
Right support	Shell Elements [kN]	Beam Elements [kN]	Diff. [kN]	Diff. [%]
x - direction	-39.7	-32.5	-7.2	22.3
y - direction	58.0	57.5	0.4	0.7

Table A.2: Reaction forces for models using shell and beam elements for a frame with beam-profiles IPE360 without haunches, both holes and outer flange restricted in translation.

Left support	Shell Elements [kN]	Beam Elements [kN]	Diff. [kN]	Diff. [%]
x - direction	39.9	32.2	7.7	21.2
y - direction	74.1	71.5	2.6	3.7
Right support	Shell Elements [kN]	Beam Elements [kN]	Diff. [kN]	Diff. [%]
x - direction	-45.7	-37.7	-8.0	21.2
y - direction	64.5	63.9	0.6	0.9

The third chosen boundary condition was to restrain all translation around the holes and translation in y -direction for both the outer and inner flange of the column. The boundaries are visualized in Fig. A.2. With this boundary condition the result of the reaction forces are presented in tables A.3 and A.4 for the two different frames.

Table A.3: Reaction forces for models using shell and beam elements for a frame with beam-profiles IPE240 with haunches, both holes and outer flange restricted in translation.

Left support	Shell Elements [kN]	Beam Elements [kN]	Diff. [kN]	Diff. [%]
x - direction	38.7	26.5	12.2	46.0
y - direction	67.1	64.2	2.9	4.6
Right support	Shell Elements [kN]	Beam Elements [kN]	Diff. [kN]	Diff. [%]
x - direction	-45.5	-33.5	-13.1	40.3
y - direction	57.5	57.5	-0.1	0.1

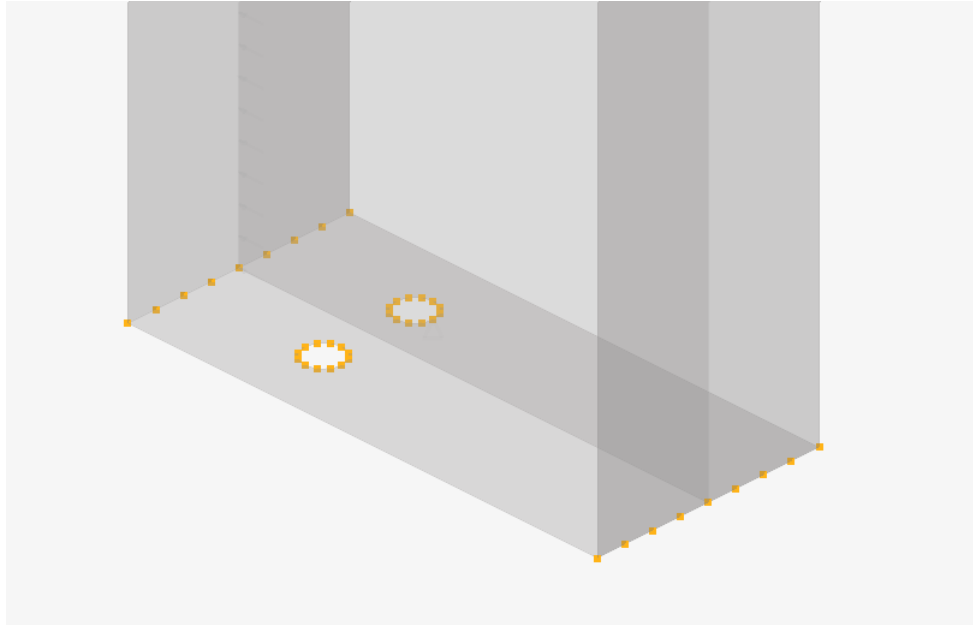


Figure A.2: Clarification of the third boundary conditions. Translation in all directions are constrained around the holes and translation in y-direction is constrained for the outer and inner flange.

Table A.4: Reaction forces for models using shell and beam elements for a frame with beam-profiles IPE360 without haunches, both holes and outer flange restricted in translation.

Left support	Shell Elements [kN]	Beam Elements [kN]	Diff. [kN]	Diff. [%]
x - direction	55.6	32.2	23.4	72.6
y - direction	74.8	71.5	3.3	4.7
Right support	Shell Elements [kN]	Beam Elements [kN]	Diff. [kN]	Diff. [%]
x - direction	-61.4	-37.7	-23.7	63.0
y - direction	63.8	63.9	-0.1	0.2

A.2 Fixed boundary condition

It is possible to build steel frames with rigid column-to-ground connections and there is an option in the design tool to apply this as a boundary condition to the two-dimensional model. The last chosen boundary condition for the three-dimensional model that was examined if it was similar to the pinned boundary conditions in the two-dimensional model was compared again with fixed boundary conditions. The comparison is shown in tables A.5 and A.6.

Table A.5: Third boundary condition compared with fixed boundary conditions applied to the two-dimensional model for frame with beam-profiles IPE240.

Left support	Shell Elements [kN]	Beam Elements [kN]	Diff. [kN]	Diff. [%]
x - direction	38.7	38.5	0.2	0.5
y - direction	67.1	65.4	1.7	2.6
Right support	Shell Elements [kN]	Beam Elements [kN]	Diff. [kN]	Diff. [%]
x - direction	-45.5	-44.5	-1.0	2.2%
y - direction	57.5	56.3	-0.1	0.1%

Table A.6: Third boundary condition compared with fixed boundary conditions applied to the two-dimensional model for frame with beam-profiles IPE360.

Left support	Shell Elements [kN]	Beam Elements [kN]	Diff. [kN]	Diff. [%]
x - direction	55.6	52.7	2.9	5.5
y - direction	74.8	72.6	2.2	3.0
Right support	Shell Elements [kN]	Beam Elements [kN]	Diff. [kN]	Diff. [%]
x - direction	-61.4	-58.2	-3.2	5.5
y - direction	63.8	62.8	-1.0	1.6